Transition to chaos of thermocapillary convection

Qi Kang,[1,2,*,†] Jia Wang,[1,*] Li Duan,[1,2,†] Xiang Li,[3] Liang Hu,[1] Lujun Li,[1] Shuoting Zhang,[1] Di Wu,[1] Pu Zhang,[1] and Wenrui Hu[1,2]

[1]*Key Laboratory of Microgravity, Institute of Mechanics, Chinese Academy of Sciences, Beijing 100190, People's Republic of China*
[2]*School of Engineering Sciences, University of Chinese Academy of Sciences, Beijing 100049, People's Republic of China*
[3]*Technology and Engineering Center for Space Utilization, Chinese Academy of Sciences, Beijing 100094, People's Republic of China*

(Received 8 October 2021; accepted 30 June 2022; published 16 September 2022)

Thermocapillary convection is a common flow in space. Experiments regarding thermocapillary convection were previously carried out in a large-scale liquid bridge with a diameter of 20 mm on the Tiangong-2 space station, and the transition process to chaos was systematically studied. Under microgravity conditions, gravity is greatly weakened, and the transition process of the flow is very slow. This allows for the opportunity to study the bifurcation process in detail. It has been found that there are abundant nonlinear physical phenomena associated with the changing geometric parameters in thermocapillary convection systems. The transition mechanisms interact with each other, leading to various transition routes. The phase space trajectories, the Lyapunov exponents, and correlation dimensions are calculated to distinguish the chaotic state under a variety of conditions. Through the chaotic dynamics analysis, the chaotic characteristics of the entire transition process are quantitatively discussed.

DOI: 10.1103/PhysRevE.106.035103

I. INTRODUCTION

Transitions are a significant characteristic of thermocapillary convection in liquid bridges. A liquid bridge refers to some liquid which is kept between two coaxial disks by surface tension. When there is a certain temperature difference between these two disks, thermocapillary convection will emerge in the zone due to Marangoni effects [1]. The flow state may transit from a steady axisymmetric flow to an oscillatory flow if the temperature difference is beyond a certain threshold and will eventually become chaotic under a large temperature difference by successive bifurcations [2]. In recent years, transitions have aroused a great deal of interest due to their impact in high-quality single crystal growth [3]. Moreover, transitions are a good physical model for the nonlinear instability of hydrodynamics [4].

Previous studies have focused on the critical instability of oscillatory flow in liquid bridges. Xu and Davis proposed that the oscillation was caused by hydrothermal waves [5]. They predicted the critical conditions and oblique propagating directions using a linear stability analysis method. However, the height of the liquid bridge is limited under normal gravity, which also confines the observation of the axial propagating wave. Therefore, scientists actively carry out space experiments under microgravity conditions. The experiments in sounding rockets [6] and on the International Space Station [7] have validated the existence of hydrothermal waves, and neutral stability curves with different aspect ratio have been obtained. Furthermore, Shevtsova *et al.* found a mode of hydrothermal wave with $m = 0$, which is an axial running wave with an axial included angle of 0 [8–9].

Beyond the critical condition, thermocapillary convection displays many nonlinear and chaotic characteristics, including spatiotemporal chaos, flow mode transition, and pattern dynamics [10–16]. The research revealed that the thermocapillary flow will experience multiple transitions and develop into spatiotemporal chaos as temperature differences continue to increase. However, the mechanism of the supercritical transition remains an open question. It has been determined that the thermocapillary flows in high supercritical states are characterized by spatiotemporal chaos (also referred to as "weak turbulence"), which is a stochastic time-dependent flow state with a slow timescale [17]. Those perspectives could be utilized to study nonlinear unsteady flow in liquid bridges.

The "routes to chaos" prescribe the transition process during the supercritical condition, which is an important topic in chaos theory. There are three typical routes to chaos: (1) subharmonic bifurcation, which is also known as period doubling bifurcation [18]. The most classic case is that the dominant frequency f of the periodic oscillation changes to f, $f/2$, then to f, $f/4$, $2f/4$, $3f/4$, …, and finally transits to chaos. The ratio of critical parameters in that transition sequence approximates the Feigenbaum constant. (2) Intermittency, which is a saddle node bifurcation. The flow alternates between periodic and chaotic motions, and then finally enters chaos. (3) The Ruelle-Takens-Newhouse route [19]. Landau believed that a system enters chaos only when there are infinite incommensurate fundamental frequencies [20]. Meanwhile, Ruelle *et al.* pointed out that quasiperiodic oscillations will enter chaos when three incommensurate frequencies appear [19].

Many transition routes are found in hydrodynamic systems. As early as 1980, Gollub and Benson experimentally

*These authors contributed equally to this work.
†Corresponding authors: kq@imech.ac.cn; duanli@imech.ac.cn

studied the transition process of Rayleigh-Bénard convection from laminar to turbulent flow and observed several transition routes [18]. Those routes included double-periodic transition, intermittent transition, and quasiperiodic transition. Smorodin *et al.* [21] studied the pattern formation in a binary-mixture layer with negative Soret coupling, which the chaotic regimes involving transitions between the subharmonic modes and the standing wave and traveling wave. In the electroconvection system, Smorodin and Taraut analyzed the nonlinear interaction of the standing wave, traveling wave, and spatiotemporal chaotic wave [22]. Kawamura *et al.* [23] and Li *et al.* [24] researched that the aspect ratios and Prandtl numbers could lead to different quasiperiodic or double-periodic transition routes. It has also been found that changes in the spatial distributions of temperature and velocity fields may cause abnormalities in transition routes, thereby leading to chaos [25]. In 2013, Zhu *et al.* [26] discovered two transition routes of double-periodic transition and quasiperiodic transition in experiments regarding thin layer flow and confirmed the transition of thermocapillary convection from temporal chaos to spatiotemporal chaos based on the fractal theory. The relationship between the fundamental frequency of the temperature oscillation and the Marangoni number was analyzed. Then, based on the fractal theory, they performed analyses of the chaotic dynamics of transition processes. In the experiments conducted under microgravity conditions on the SJ-10 satellite, the transition phenomena leading to chaos in thermocapillary convection were observed [27]. It was found that there were different transition routes in the transforming process of the flowing mode [28].

In the thermocapillary convection of liquid bridges, the transition routes in chaos theory have been observed, including the double-periodic route and the quasiperiodic route. Hu *et al.* theoretically studied that there was a double-periodic route in small-scale liquid bridges, and its bifurcation condition conformed to the universal Feigenbaum constant [29]. Based on analyzing the effects of environmental conditions on the flow instability, Melnikov *et al.* [30] determined that the flow usually took the quasiperiodic transition route under different external airflow conditions. Through a spectrogram, Yasnou *et al.* clearly observed the periodic oscillation and quasiperiodic oscillation with two frequencies and quasiperiodic oscillation with three frequencies [16]. Gaponenko *et al.* further discussed the effect of the gas temperature on the wave mode selection and nonlinear evolution of the hydrothermal wave [31]. Frank and Schwabe observed the transitions of the spatiotemporal structures of thermocapillary convection in half-floating zone liquid bridges with different working fluids [13]. They also analyzed the quasiperiodic and double-periodic transition routes in the spatial structure of the flow field. Aa *et al.* [32] observed classic second transition processes and jumping behaviors in the convection through experimental and theoretical investigations. Wang *et al.* [33] observed a variety of transition phenomena in large-scale liquid bridges and identified a transition route in which the double-periodic oscillation was coupled with the quasiperiodic oscillation.

Several advantages have been found in studying the transition processes of liquid bridge thermocapillary convection in space experiments, as follows:

(1) *Reducing the influence of gravity on thermocapillary convection*: First, buoyancy convection is excluded in experiments conducted in space. Second, air convection and thermal noise are restrained.

(2) *Establishing various liquid bridges to enrich transition routes*: Experiments conducted on the ground are confined to specific geometric parameters due to the height limitations of liquid bridges. Experiments conducted in space can greatly expand the range of the geometric parameters of liquid bridges, which increases the opportunity to find more transition routes.

(3) *Large Marangoni numbers*: The Marangoni number of a liquid bridge is directly proportional to the size of the liquid bridge, and chaotic processes are easier to observe in large-scale liquid bridges. Previous experiments conducted in space regarding the transition of thermocapillary convection have acquired fruitful achievements. For example, Japan has carried out experiments on thermocapillary convection in liquid bridges on the International Space Station in order to explore the structures of flow fields, especially under the conditions of large temperature differences [34]. From 2016 to 2019, the Tiangong-2 (TG-2) Liquid Bridge Space Experiment Project took the bifurcations of thermocapillary convection and transition routes to chaos as innovative research projects [35,36].

More than 740 groups of experiments have been carried out in the Tiangong-2 space laboratory, and a large amount of valuable data has been obtained. The results have confirmed that the thermocapillary of liquid bridges displayed distinctive flow patterns and significant nonlinear characteristics. The transition routes were categorized by the temperature oscillation signals obtained from the liquid bridge, and a variety of characteristic transition phenomena under microgravity conditions were observed. By introducing attractors, it was able to describe the chaotic motion of the thermocapillary convection. In addition, using the theory of chaotic dynamics, the correlation dimension and Lyapunov exponent were calculated based on the reconstruction of phase space for the purpose of distinguishing the chaotic state and analyzing the entire transition process.

II. EXPERIMENTAL EQUIPMENT

The experimental model was introduced by Kang *et al.* in 2019 [35], as shown in Fig. 1. Both of the bridge columns are made of copper. One bridge column is heated by electrothermal film to T_H, while the other column is maintained at T_L by a thermoelectric cooler. When a temperature difference ΔT ($\Delta T = T_H - T_L$) is applied, convection is observed to occur inside the liquid zone. Once the temperature difference exceeds a certain threshold value (ΔT_c), the convection becomes unstable and transfers into oscillatory flow. In addition, as the temperature difference increases, it finally develops into chaos or even turbulent flow. The temperature heating rate involved here is 0.3 °C per minute, and the initial temperature difference is 0 °C. When the ΔT reaches a predetermined value, the system maintains the current high-temperature and low-temperature values, as detailed in Fig. 2.

Five thermocouples (1 to 5) are used to measure the temperature inside the liquid bridge, and the temperatures of the cold column and the heat column are measured by two other

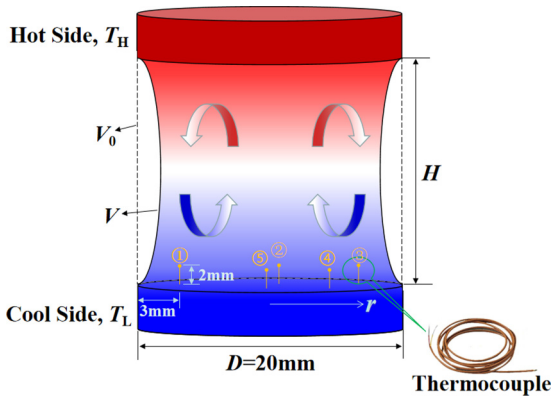

FIG. 1. Liquid bridge model.

thermocouples, respectively. The thermocouples used in the experiments are K-type, with diameters of 0.02 mm. The successive included angles of the five thermocouples are 0°, 90°, 180°, 270°, and 315°, respectively. The experiments showed that the onset and transitions of each thermocouple signals happened at the same time. Though there are phase differences, the spectra of the thermocouples (1 to 5) are consistent. Therefore, thermocouple no. 2 is chosen for further discussion (Fig. 2).

KF96L 5cSt silicone oil (Pr = 67.29; thermal diffusion coefficient $\kappa = 0.12\,\mathrm{m^2 s^{-1}}$; surface tension coefficient $\sigma_T = 6.58\times10^{-5}\,\mathrm{N\,m^{-1}\,K^{-1}}$; density $\rho = 915\,\mathrm{kg\,m^{-3}}$; kinematic viscosity $\nu = 5\times10^{-6}\,\mathrm{m^2 s^{-1}}$) is chosen as the experimental working fluid. The silicone oil is stored in a liquid cylinder, and a piston in the cylinder is used to inject or suck out the silicon oil to build a liquid bridge. The movement of piston is driven by a motor from power integrations (PI) company, which allows for the precise control of the volume ratio of the liquid bridge.

A number of dimensionless parameters, including the geometric parameters A and V, along with some physical properties of the fluid are introduced for the purpose of characterizing the flow and examining their impacts on the flow. The range of volume ratio V is [0.54 to 1.15], and the range of the aspect ratio A was [0.3 to 1.1], as detailed below.

Aspect ratio: $A = \frac{H}{D}$, where H is the height of the liquid bridge, and the diameter of the liquid bridge column is $D = 20$ mm.

Volume ratio: $V = \frac{V_l}{V_0}$, where V_0 represents the volume of the gap between two cylinders, and V_l indicates the volume of the experimental working fluid.

Marangoni number: $\mathrm{Ma} = \frac{|\sigma_T|\Delta T H}{\rho\nu\alpha} = \mathrm{Pr\,Re}$, which characterizes the ratio of the heat transport caused by thermocapillary convection to the heat transport caused by heat conduction. The critical Marangoni number corresponding to the critical temperature difference ΔT_c is recorded as $\mathrm{Ma_c}$.

The temperature dependency of the kinematic viscosity of the working fluid is evaluated from the following equations:

$$\frac{\upsilon}{\upsilon_{25}} = \exp\left(5.892\frac{25-T}{273.15+T}\right), \tag{2.1}$$

$$\upsilon = \frac{\upsilon(T_H)+\upsilon(T_L)}{2}, \tag{2.2}$$

where $\upsilon_2 5$ and T are the kinematic viscosity at 25 °C and the temperature considered, respectively.

The spectrogram and power spectra are used to analyze the oscillation signals of thermocapillary convection. The long-term trends of the signals are removed prior to conducting the spectrum analysis, which can obtain the oscillatory signal of the convention. The spectrogram, applying a sequence of a widowed Fourier transform with sliding windows, gives a

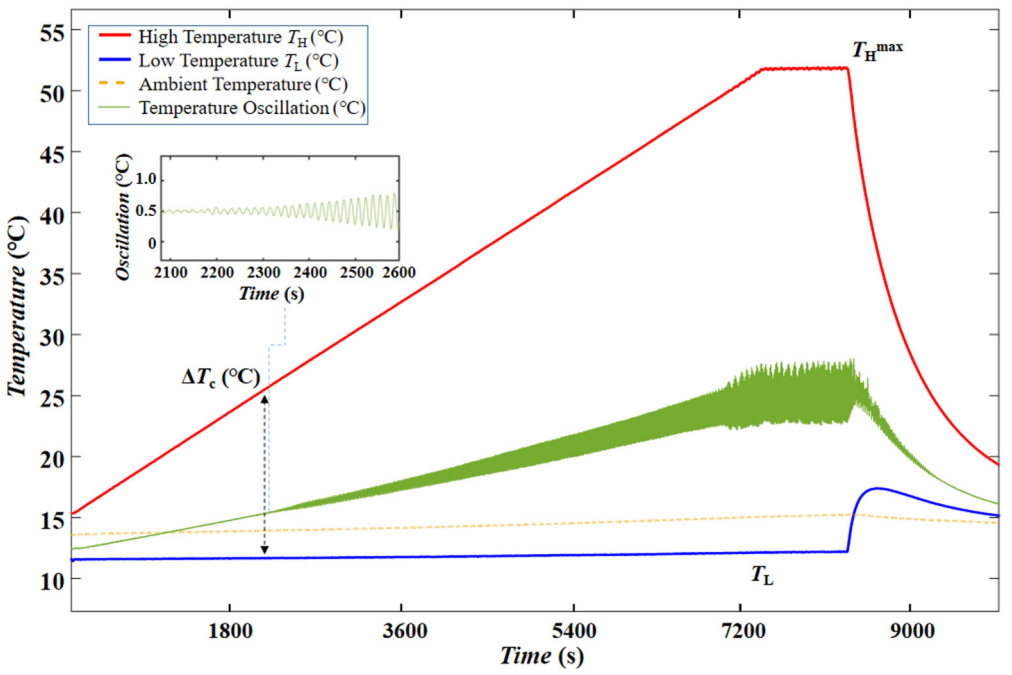

FIG. 2. Time histories of the temperature oscillations ($A = 0.8$; $V = 0.8$).

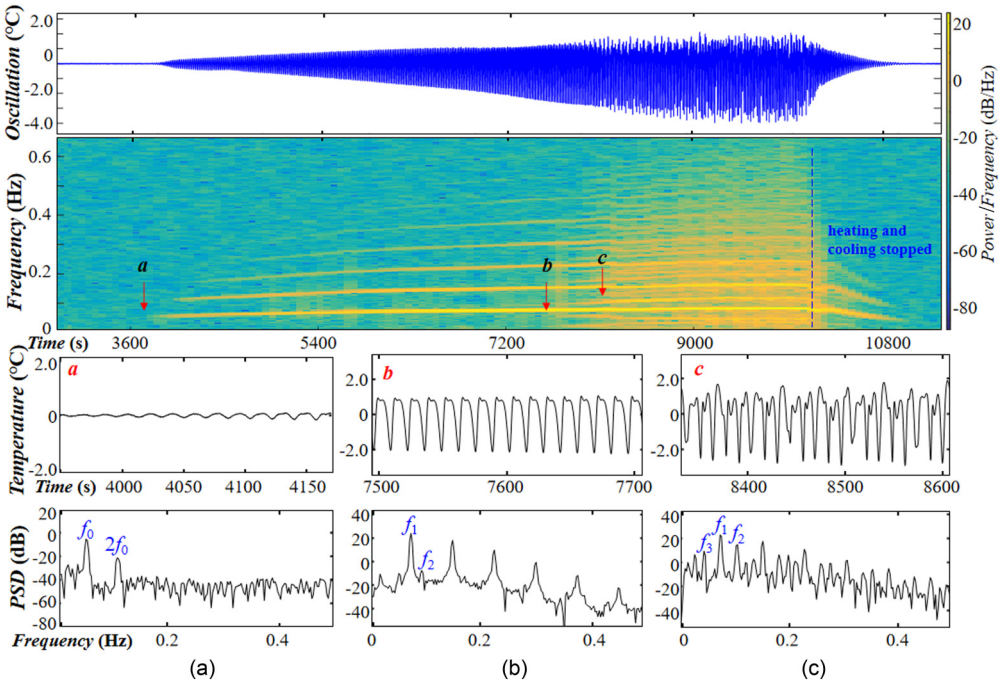

FIG. 3. RTN transition processes ($A = 0.6$; $V = 0.84$) including the temperature oscillation signals, power spectra, and corresponding power spectra at different Marangoni numbers: (a) $\mathrm{Ma}^a = \mathrm{Ma_c}$, periodic oscillation; (b) $\mathrm{Ma}^b = 2.03\,\mathrm{Ma_c}$, oscillation with two fundamental frequencies, f_1 and f_2; (c) $\mathrm{Ma}^c = 2.21\,\mathrm{Ma_c}$, oscillation with three fundamental frequencies, f_1, f_2, and f_3.

two-dimensional graph of time vs the Fourier spectrum. A hamming window can reduce the frequency spectrum leakage, and a properly increased window size can ensure the resolution in both the frequency domain and the time domain. The power spectral density can be estimated using the pWelch method, and the window will be 2048, which is equivalent to more than 100 sec.

III. EXPERIMENTAL RESULTS

A. Quasiperiodic transition process

The quasiperiodic transition route is caused by several Hopf bifurcations. Three typical quasiperiodic transition routes are concluded in the space experiments of thermocapillary convection in liquid bridges.

Type I: Ruelle-Takens-Newhouse route. The Ruelle-Takens-Newhouse route is quasiperiodic oscillation with three incommensurate frequencies and phase locking coexisting [19]. Under the conditions of an aspect ratio of $A = 0.60$, and a volume ratio of $V = 0.84$, the flow loses stability and transferred from a steady state to an oscillating state at $\mathrm{Ma} = \mathrm{Ma_c}$ (point a; $t = 3791$ sec). This is a periodic fluctuation with a certain fundamental frequency of $f_0 = 0.054$ Hz, as shown in Fig. 3(a). Then it has been observed that with further increases in the temperature difference, at $\mathrm{Ma} = 2.03\,\mathrm{Ma_c}$ (point b; $t = 7696$ sec), the fundamental frequency has increased to $f_1 = 0.078$ Hz. The flow bifurcations exhibit the appearance of a second fundamental frequency, $f_2 = 0.110$ Hz [Fig. 3(b)]. It has been found that f_1 and f_2 are incommensurate, and there is a relationship of $f_\mathrm{L} = f_1 - f_2 = 0.032$ Hz observed. The remaining frequencies could all be linearly expressed by those two fundamental frequencies. The ratio of f_1/f_2 keeps constant during the process, and this state is referred to as frequency locking or phase locking [18], which is a classic common phenomenon in the quasiperiodic transition process. This frequency locking implies the nonlinear coupling between these two frequencies. In addition, the fundamental frequency presents an increasing trend of linear and continuous change. This relationship will be broken until the appearance of the third fundamental frequency in the temperature field ($f_1 = 0.080$ Hz; $f_2 = 0.115$ Hz; $f_3 = 0.047$ Hz) [Fig. 3(c); $t = 8378$ sec]. It has been confirmed that the classic Ruelle-Takens-Newhouse (RTN) route exhibits a transition process from quasiperiodic oscillation with three fundamental frequencies, to a chaotic state. It has been previously observed by Libchaber *et al.* [37] in mercury Bénard experiments in a magnetic field and by Martin *et al.* in experiments regarding ferroelectric barium-sodium-niobate (BSN) crystals [38]. However, it has been found that in many cases, including in ground buoyancy-thermocapillary convection systems [26,33], due to the instability of the flow, it is difficult to observe the third incommensurate frequency in which the flow becomes chaos from quasiperiodic oscillations with two fundamental frequencies. The route to chaos is similar to that in the Curry-Yorke model, where chaos appears after quasiperiodicity and phase locking occurs [39]. That transformation also belongs to the RTN route.

Type II: Quasiperiodic transition with two incommensurate frequencies. The most obvious feature of this transition route is beat phenomena. As shown in Fig. 4, the steady-state flow first transits to a periodic oscillatory flow with the frequency $f_0 = 0.098$ Hz [Fig. 4(a); point a, $t = 6061$ sec]. Then, at $\mathrm{Ma}^c = 1.28\,\mathrm{Ma_c}$, the spectrogram shows a split in the frequencies and the appearance of another two incommensurate fundamental frequencies, $f_1 = 0.111$ Hz and $f_2 = 0.153$ Hz [Fig. 4(b); point b, $t = 7758$ sec]. As can be seen

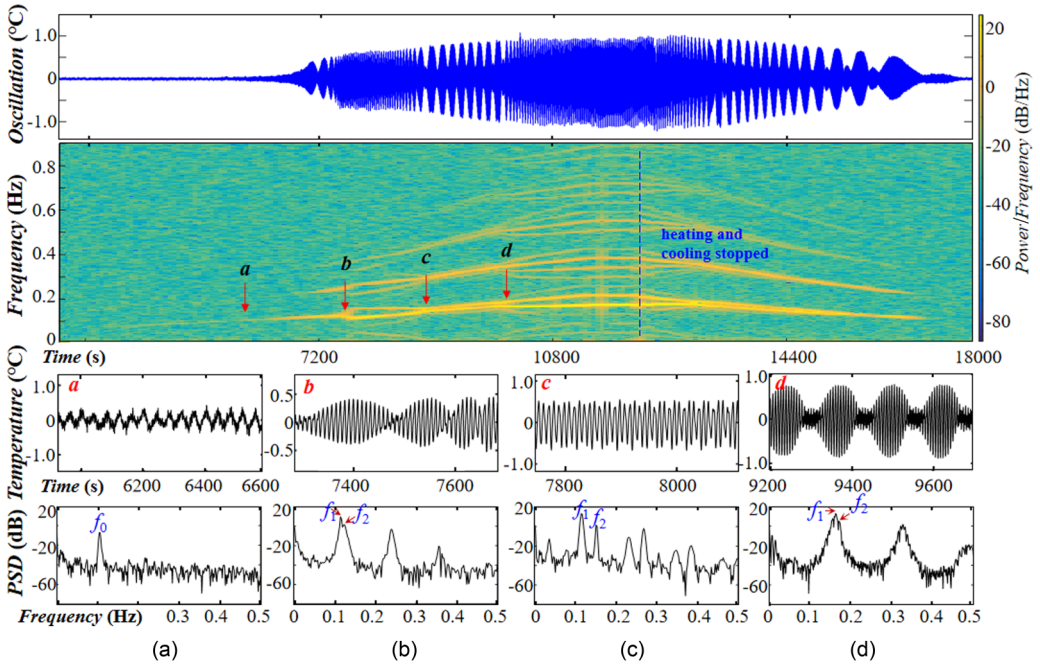

FIG. 4. Quasiperiodic transition route coupled with beat phenomenon ($A = 0.4$; $V = 0.45$) including the temperature oscillation signals, spectrogram, and segmented temperature signals, and corresponding energy spectra: (a) $\mathrm{Ma}^a = \mathrm{Ma_c}$, periodic oscillation; (b) $\mathrm{Ma}^b = 1.28\,\mathrm{Ma_c}$, oscillation with two fundamental frequencies; (c) $\mathrm{Ma}^c = 1.47\,\mathrm{Ma_c}$, oscillation with two fundamental frequencies; (d) $\mathrm{Ma}^d = 1.66\,\mathrm{Ma_c}$, oscillation with two fundamental frequencies.

in the figure, f_1 gradually increases to 0.132 Hz, while f_2 remains constant. It has been observed that at $\mathrm{Ma} = 1.47\,\mathrm{Ma_c}$, another bifurcation occurs in the flow field causing dramatic changes in the frequencies, such as $f_1 = 0.149$ Hz and $f_2 = 0.157$ Hz [Fig. 4(c); point c, $t = 8898$ sec]. However, when $\mathrm{Ma} = 1.66\,\mathrm{Ma_c}$ [Fig. 4(d); point d, $t = 10067$ sec], it has been found that f_1 and f_2 became two new frequencies once again ($f_1 = 0.161$ Hz; and $f_2 = 0.184$ Hz). When $1.47\,\mathrm{Ma_c} < \mathrm{Ma} < 1.66\,\mathrm{Ma_c}$, which is similar to the RTN route, there is a certain gap observed between these two fundamental frequencies, $f_L = f_1$-f_2. Meanwhile, with $1.28\,\mathrm{Ma_c} < \mathrm{Ma} < 1.47\,\mathrm{Ma_c}$ or $\mathrm{Ma} > 1.66\,\mathrm{Ma_c}$, the flow presents a beat phenomenon, and the amplitude point of the temperature oscillation signal forms envelopes. This is due to the fact that those two fundamental frequencies are very close in the PSD ($f_1 \approx f_2$), and the oscillating signals are superimposed on each other, thereby forming periodic fluctuations in amplitude [40].

There are two competitive or stalemate mechanisms in the aforementioned quasiperiodic transition routes. Bifurcation will lead to a change in the oscillation frequency. When there is a slight temperature disturbance in the heat dissipation system, the bifurcation will break the balanced state and enter another state, resulting in the evolution of the convection.

Type III: Quasiperiodic transition route with inverse bifurcation. As can be seen in Fig. 5, when the volume ratio is 0.56 and the aspect ratio is 1.1, the flow alternatively exhibits the motions of quasiperiodic oscillation and periodic oscillation, and the flow presents an "inverted bifurcation phenomenon." In Fig. 5(a) it can be seen that when $\mathrm{Ma} = \mathrm{Ma_c}$ (point a, $t = 2870$ sec), the flow behaves as a periodic motion ($f_1 = 0.034$ Hz). However, when $\mathrm{Ma} = 1.37\,\mathrm{Ma_c}$, the flow is quasiperiodic motion, with the fundamental frequencies of $f_1 = 0.059$ Hz and $f_2 = 0.068$ Hz, as illustrated in Fig. 5(b) (point b, $t = 3946$ sec). Thereafter, when $1.64\,\mathrm{Ma_c} < \mathrm{Ma} < 2.71\,\mathrm{Ma_c}$ or $2.71\,\mathrm{Ma_c} < \mathrm{Ma} < 3.43\,\mathrm{Ma_c}$, the periodic motion with the main frequency $f_1 = 0.061$ Hz [Fig. 5(c); point c, $t = 4716$ sec] and the quasiperiodic motion with the fundamental frequencies $f_1 = 0.093$ Hz and $f_2 = 0.110$ Hz [Fig. 5(d); point d, $t = 7790$ sec] reappears. Then, when $\mathrm{Ma} = 3.43\,\mathrm{Ma_c}$ (point e, $t = 9844$ sec), the flow finally enters chaos, as shown in Fig. 5(e).

The flow alternatively exhibits a periodic oscillation, quasiperiodic oscillation, and chaos with the increasing Marangoni number, as detailed in Fig. 6. Then, at $\mathrm{Ma} = 1.73\,\mathrm{Ma_c}$, the flow field displays a quasiperiodic oscillation with the fundamental frequencies ($f_1 = 0.041$ Hz and $f_2 = 0.027$ Hz, point b, $t = 4100$ sec) and became chaos at $\mathrm{Ma} = 2.28\,\mathrm{Ma_c}$ (point c, $t = 5332$ sec). At $\mathrm{Ma} = 3.67\,\mathrm{Ma_c}$ (point d, $t = 8698$ sec), it transits to periodic motion once again and eventually enters chaos at $\mathrm{Ma} = 4.50\,\mathrm{Ma_c}$ (point e; $t = 10665$ sec). In the Rayleigh-Bénard convection, Paul *et al.* has regarded the conversion from triple-periodic motion to periodic motion as "crisis" [41]. The phenomenon in which the flow state transits into a less complicated flow is referred to as "reverse bifurcation phenomenon."

B. Double-periodic transition process

The double-periodic transition route is a subharmonic bifurcation model proposed by Feigenbaum [32]. In the space experiments, the double-periodic transition routes are divided into three categories.

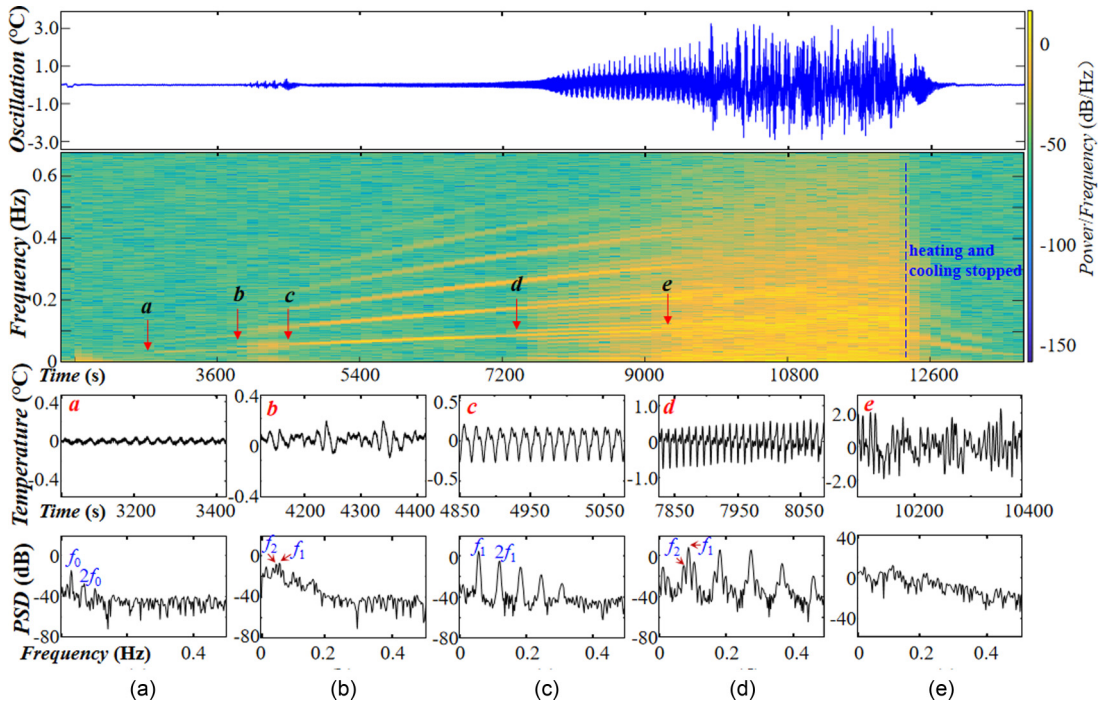

FIG. 5. Quasiperiodic transition route coupled with reverse bifurcation ($A = 1.1$; $V = 0.56$) including the temperature oscillation signals, spectrogram, zoom of the temperature signals, and the corresponding energy spectra: (a) $\mathrm{Ma}^a = \mathrm{Ma_c}$, periodic oscillation; (b) $\mathrm{Ma}^b = 1.37\,\mathrm{Ma_c}$, quasiperiodic oscillation with two fundamental frequencies; (c) $\mathrm{Ma}^c = 1.64\,\mathrm{Ma_c}$, periodic oscillation; (d) $\mathrm{Ma}^d = 2.71\,\mathrm{Ma_c}$, quasiperiodic oscillation with two fundamental frequencies; (e) $\mathrm{Ma}^e = 3.43\,\mathrm{Ma_c}$, chaos.

Type I: Feigenbaum route. The Feigenbaum route means that the periodic state transits by successive doubling period bifurcations. In thermocapillary convection with an aspect ratio of 0.65 and a volume ratio of 0.65, when $\mathrm{Ma_c} < \mathrm{Ma} < 1.89\,\mathrm{Ma_c}$, the temperature in the time domain will perform a sine oscillation with a frequency of $f_0 = 0.068$ Hz [Fig. 7(a); $t = 5022$ sec; point *a*]. In the spectrogram, an infinitely narrow peak can be seen at the point corresponding

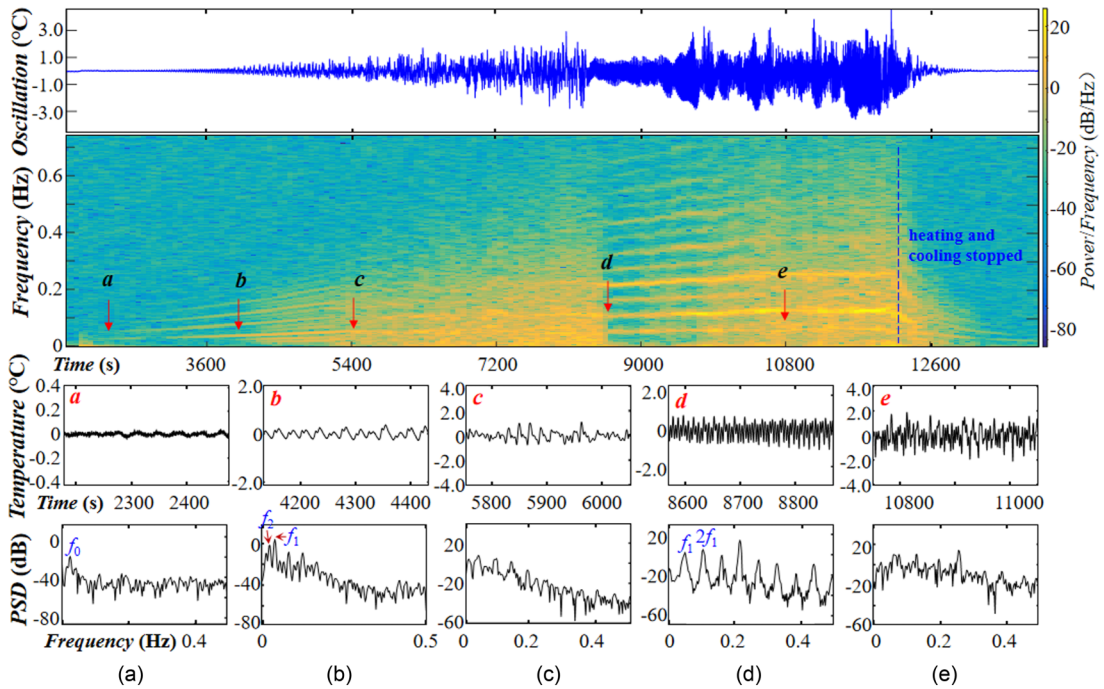

FIG. 6. Quasiperiodic transition route coupled with reverse bifurcation ($A = 1.1$; $V = 0.66$): (a) $\mathrm{Ma}^a = \mathrm{Ma_c}$, periodic oscillation; (b) $\mathrm{Ma}^b = 1.73\,\mathrm{Ma_c}$, quasiperiodic oscillation; (c) $\mathrm{Ma}^c = 2.28\,\mathrm{Ma_c}$, chaos; (d) $\mathrm{Ma}^d = 3.67\,\mathrm{Ma_c}$, periodic oscillation; (e) $\mathrm{Ma}^e = 4.50\,\mathrm{Ma_c}$, chaos.

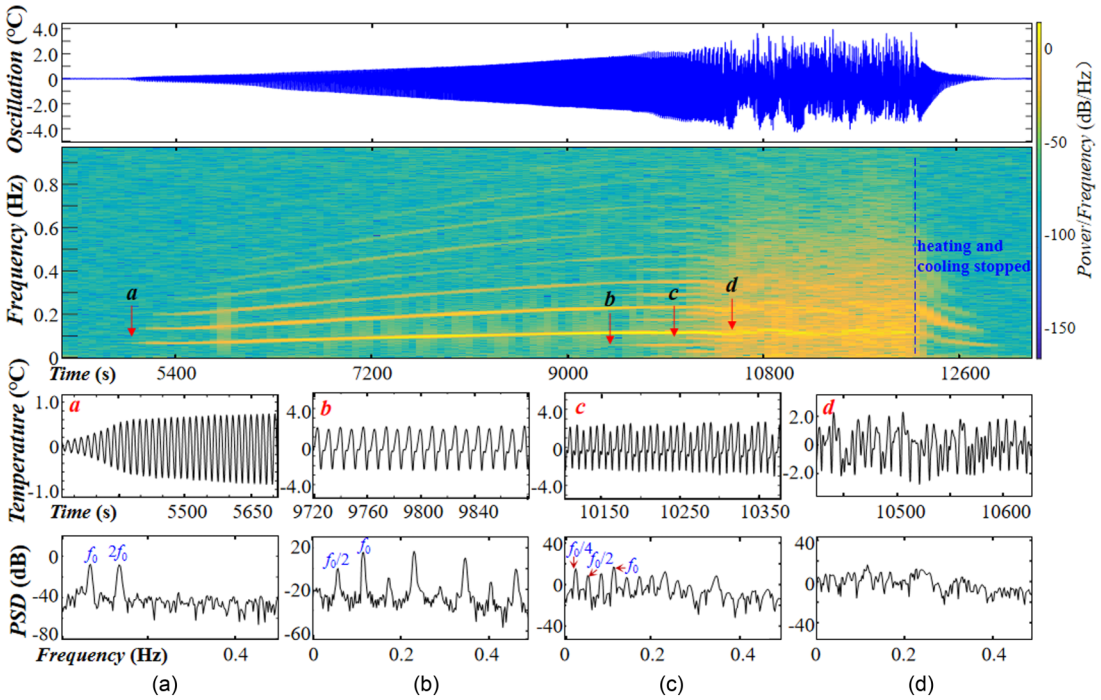

FIG. 7. Feigenbaum transition route ($A = 0.65$; $V = 0.65$): (a) $\mathrm{Ma}^a = \mathrm{Ma_c}$, periodic oscillation; (b) $\mathrm{Ma}^b = 1.89\,\mathrm{Ma_c}$, double-periodic oscillation; (c) $\mathrm{Ma}^c = 1.98\,\mathrm{Ma_c}$, quadruple-periodic oscillation; (d) $\mathrm{Ma}^d = 2.07\,\mathrm{Ma_c}$, chaos.

to the independent variable f, and the height of the peak represents the intensity (power) of the frequency component. When $\mathrm{Ma} = 1.89\,\mathrm{Ma_c}$ [Fig. 7(b); $t = 9482$ sec; point b], in addition to the original spectrum peak at $f_1 = 0.117$ Hz, a new spectrum peak component ($f_1/2$) appears. When $\mathrm{Ma} = 1.98\,\mathrm{Ma_c}$ ($t = 9943$ sec; point c), the flow bifurcates once again, and two new spectrum peaks (corresponding to $f_1/4$ and $3f_1/4$) appear in the power spectrum. However, when $\mathrm{Ma} > 1.98\,\mathrm{Ma_c}$, the power spectrum transits from a separated spectrum to a continuous indivisible spectrum. Meanwhile, the flow enters a broadband chaotic motion with a noisy background, as shown in Fig. 7(d) ($t = 10404$ sec; point d). In the current study, the critical temperature differences at which the flow bifurcated are selected, and the corresponding Feigenbaum constant $\delta_1 = (\Delta T_{f1/2} - \Delta T_{f0})/(\Delta T_{f1/4} - \Delta T_{f1/2}) = (39.27-19.35)/(43.54-39.27) = 4.67 \pm 0.02$ is obtained, which is close to the theoretical value and conforms to Feigenbaum's universal law as follows:

$$\delta = \lim_{n\to\infty} \frac{a_n - a_{n-1}}{a_{n+1} - a_n} = 4.6692016. \tag{3.1}$$

Type II: The multiple-periodic transition route. The bifurcation occurs in the above-mentioned Feigenbaum route with the period being doubled, which means that the period (p) bifurcates into $p \times 2^n$ ($n = 1, 2, 3, \ldots$) in succession. Similarly, bifurcations in which the period is tripled to $p \times 3^n$ (Fig. 8), quadrupled to $p \times 4^n$ (Fig. 9) or multiplied to $p \times k$ ($k = 2, 3, 4, 5, \ldots$), appearing in some specific bifurcation regions with different Feigenbaum constants, which are also found to be universal [29].

Due to the lack of gravity in space environments, a tiny disturbance in the experimental system will affect convection systems dominated by surface tension. In this study, the liquid bridge with an aspect ratio of $A = 0.5$, and a volume ratio of $V = 0.82$, (Fig. 10), the flow transits from a steady state to periodic oscillation when the Marangoni number exceeds the threshold (point a, $t = 4561$ sec). However, when $\mathrm{Ma} = 2.19\,\mathrm{Ma_c}$ (point b, $t = 9634$ sec), quartered frequencies $nf_1/4$ ($n = 1, 2, 3, \ldots$) appear in the spectrogram, which indicates that the flow had entered quadruple-periodic motion. It is interesting to note that, differing from the previous results shown in Figs. 7 to 9, k is no longer a constant number in the subharmonic bifurcations transition process, and it can change from an even number to an odd number. When $\mathrm{Ma} = 2.36\,\mathrm{Ma_c}$ (point c, $t = 10381$ sec), quintuple frequencies $nf_1/5$ ($n = 1, 2, 3, \ldots$) appear in the spectrogram, and the flow behaves as quintuple-periodic motion. The conversion between those two subharmonic periodic modes is the flow transition caused by the bifurcations of the flow field.

Type III: Subharmonic transition process with inverse bifurcation. Under the conditions of a volume ratio V of 0.98 and an aspect ratio A of 0.95 (Fig. 11), it has been found that the flow evolves following the route as follows: steady-state to periodic oscillation to triple-periodic oscillation to sixfold-periodic oscillation ($n = 1, 2, 3, \ldots$). However, when $\mathrm{Ma} = 2.49\,\mathrm{Ma_c}$ (point d, $t = 9172$ sec), the flow suddenly transits into triple-periodic oscillation from sixfold-periodic oscillation, with the emergence of the inverse period-doubling bifurcation. Then, when $\mathrm{Ma} = 2.63\,\mathrm{Ma_c}$ (point e; $t = 9688$ sec), the flow no longer continues to bifurcate, suddenly loses its regularity, and enters chaos. When the volume ratio V is 0.70 and aspect ratio A is 0.85 (Fig. 12), the flow directly transits from periodic motion into sixfold-periodic motion at $\mathrm{Ma} = 2.06\,\mathrm{Ma_c}$ (point b, $t = 9274$ sec).

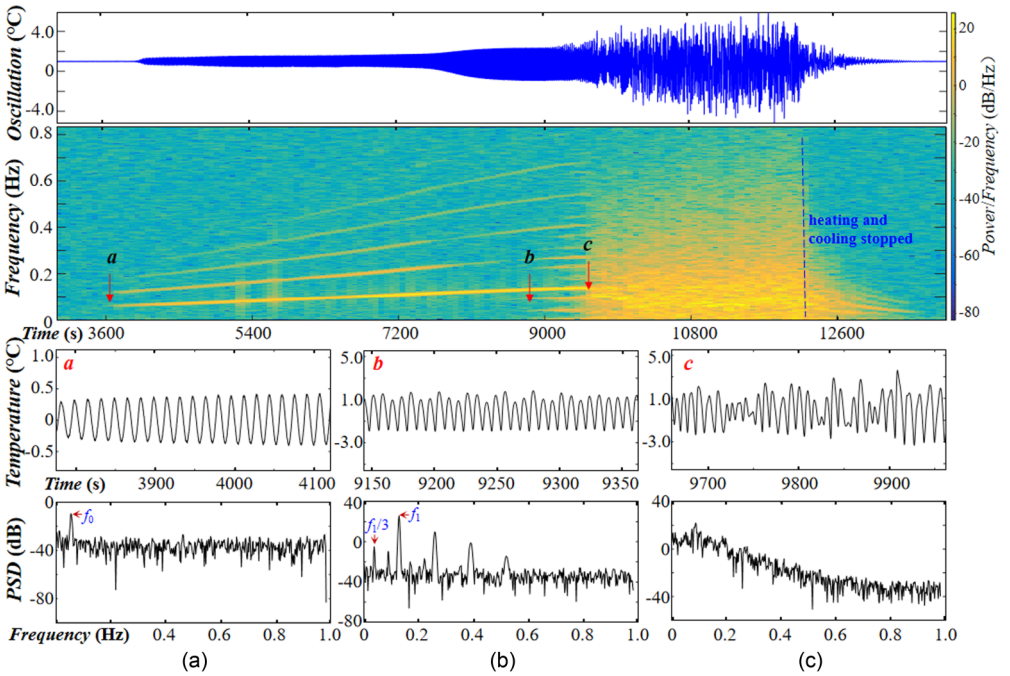

FIG. 8. Triple-periodic transition route ($A = 0.95$; $V = 0.94$): (a) $\mathrm{Ma}^a = \mathrm{Ma}_c$, periodic oscillation; (b) $\mathrm{Ma}^b = 2.38\,\mathrm{Ma}_c$, triple-periodic oscillation; (c) $\mathrm{Ma}^c = 2.61\,\mathrm{Ma}_c$, chaos.

Then it transits into triple-periodic motion through the inverse bifurcation at $\mathrm{Ma} = 2.22\,\mathrm{Ma}_c$ (point c, $t = 10008$ sec) and eventually becomes chaos at $\mathrm{Ma} = 2.34\,\mathrm{Ma}_c$ (point d, $t = 10528$ sec).

The mechanism of chaos is complicated, and a transition route will reflect only one aspect. The three transition processes shown in Figs. 13 to 15 are coupled with periodic motion. As shown in Fig. 13, the flow transits from double-periodic oscillation back into periodic motion with $f = 0.088$, Hz at $\mathrm{Ma} = 2.01\,\mathrm{Ma}_c$ (point c, $t = 6487$ sec) and then maintains that state for a considerable length of time. The flow transits into quadruple-periodic motion through a bifurcation at $\mathrm{Ma} = 3.00\,\mathrm{Ma}_c$ (point d, $t = 8475$ sec) and finally enters a chaotic state at $\mathrm{Ma} = 3.16\,\mathrm{Ma}_c$ (point e, $t = 10201$ sec).

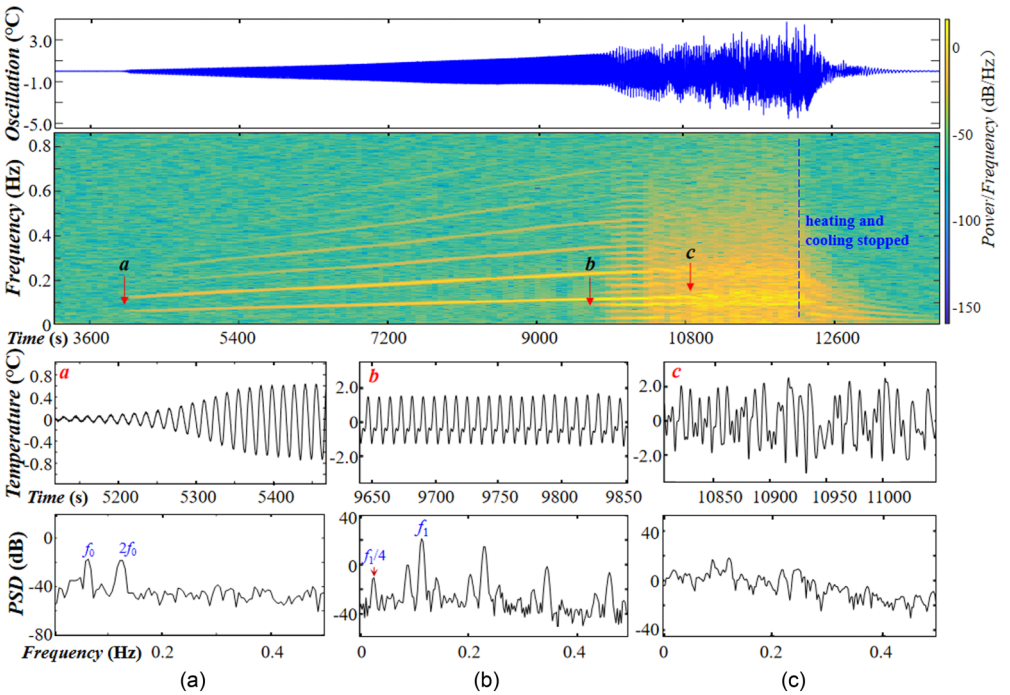

FIG. 9. Quadruple-periodic transition route ($A = 0.85$; $V = 0.78$): (a) $\mathrm{Ma}^a = \mathrm{Ma}_c$, periodic oscillation; (b) $\mathrm{Ma}^b = 2.44\,\mathrm{Ma}_c$, quadruple-periodic oscillation; (c) $\mathrm{Ma}^c = 2.71\,\mathrm{Ma}_c$, chaos.

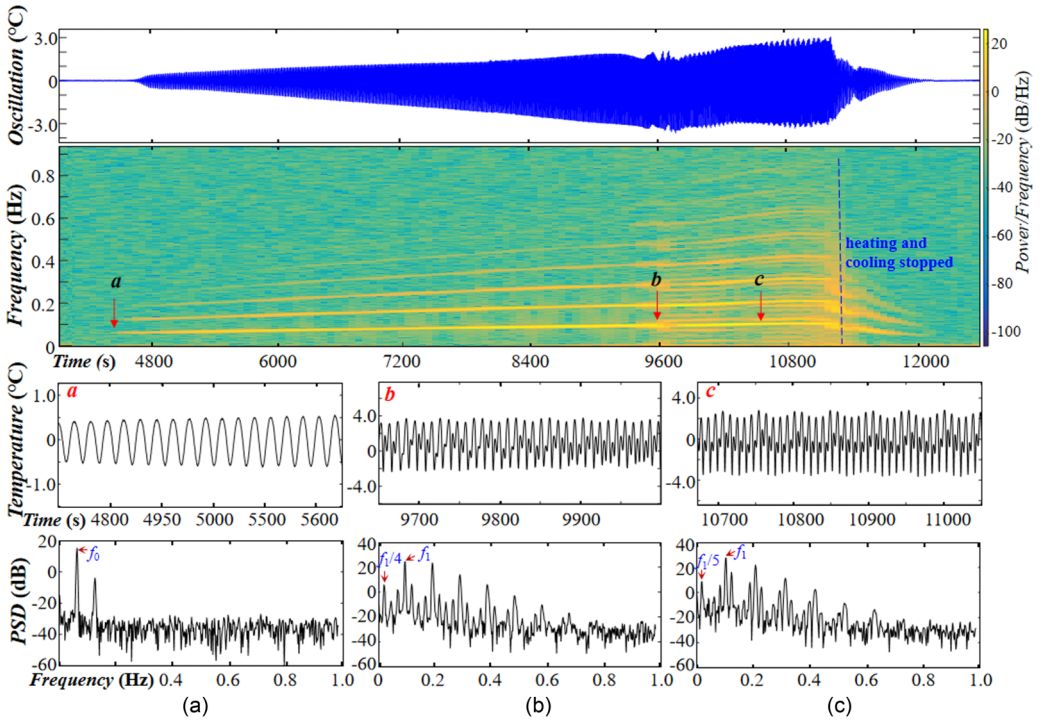

FIG. 10. Double-periodic transition route from quadruple-periodic oscillation to quintuple-periodic oscillation ($A = 0.5$; $V = 0.82$): (a) $\mathrm{Ma}^a = \mathrm{Ma_c}$, periodic oscillation; (b) $\mathrm{Ma}^b = 2.19\,\mathrm{Ma_c}$, quadruple-periodic oscillation; (c) $\mathrm{Ma}^c = 2.36\,\mathrm{Ma_c}$, quintuple-periodic oscillation.

Similar to the transition route detailed in Fig. 10, the double-periodic motion could potentially bifurcate into a k-periodic oscillation ($k \neq 2$) during the transition process. As shown in Figs. 14 and 15, the periodic motion occurring at a later regime can transition to triple- or quintuple-periodic motion by bifurcations ($n = 1, 2, 3, \ldots$), and the flow will potentially alternate between periodic motion and k-periodic motion ($k = 2, 3, 4, \ldots$).

This inverse phenomenon includes the following processes: periodic oscillation, double-periodic oscillation,

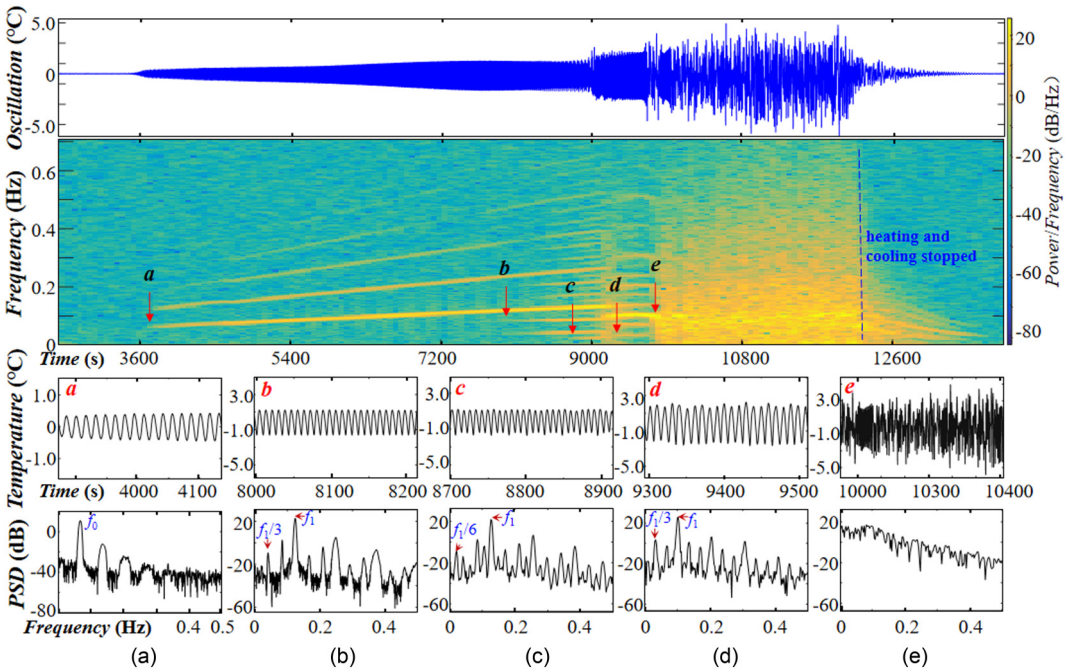

FIG. 11. Double-periodic transition route with inverse bifurcation I ($A = 0.95$; $V = 0.98$): (a) $\mathrm{Ma}^a = \mathrm{Ma_c}$, periodic oscillation; (b) $\mathrm{Ma}^b = 2.12\,\mathrm{Ma_c}$, triple-periodic oscillation; (c) $\mathrm{Ma}^c = 2.33\,\mathrm{Ma_c}$, sixfold-periodic oscillation; (d) $\mathrm{Ma}^d = 2.49\,\mathrm{Ma_c}$, triple-periodic oscillation; (e) $\mathrm{Ma}^e = 2.63\,\mathrm{Ma_c}$, chaos.

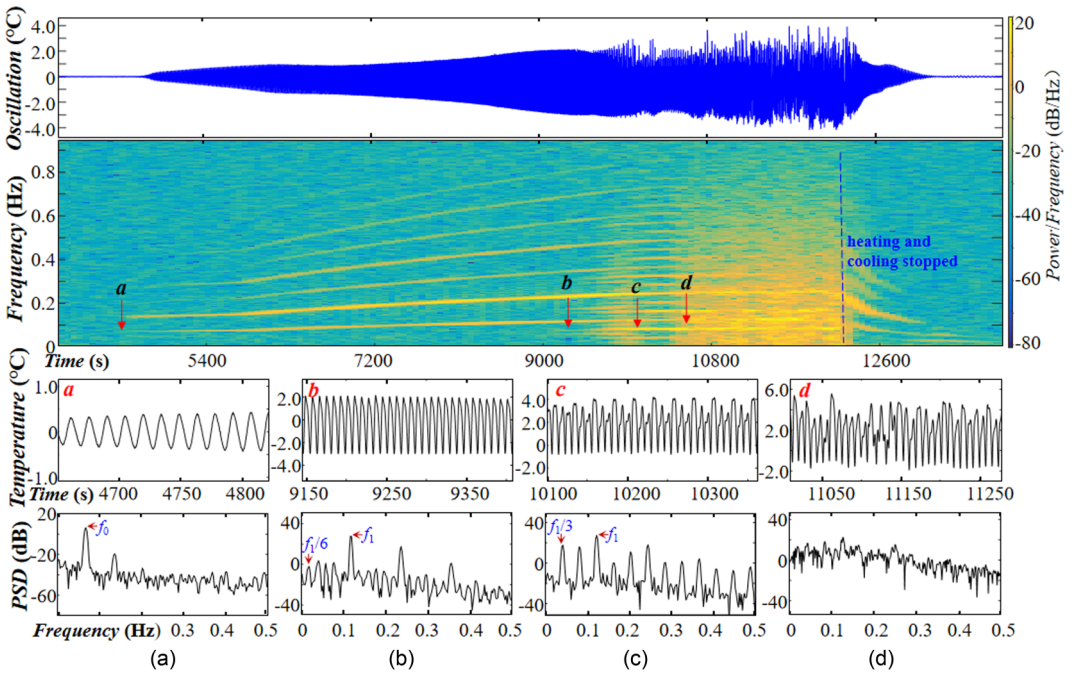

FIG. 12. Double-periodic transition route with inverse bifurcation II ($A = 0.85$; $V = 0.70$): (a) $\mathrm{Ma}^a = \mathrm{Ma_c}$, periodic oscillation; (b) $\mathrm{Ma}^b = 2.06\,\mathrm{Ma_c}$, sixfold-periodic oscillation; (c) $\mathrm{Ma}^c = 2.22\,\mathrm{Ma_c}$, triple-periodic oscillation; (d) $\mathrm{Ma}^d = 2.34\,\mathrm{Ma_c}$, chaos.

periodic oscillation, and double-periodic oscillation, respectively, and does not comply with Feigenbaum's period-doubling bifurcation model. Not all of the period-doubling transition routes are included in the processes during which the flow bifurcates with the period being continuously doubled before entering chaos. Therefore, Feigenbaum's period-doubling bifurcation model is considered to be an ideal model.

C. Coupling transition processes

As can be seen in Fig. 16, the flow experiences quadruple-periodic motion after two bifurcations. However, at $\mathrm{Ma} = 2.33\,\mathrm{Ma_c}$ (point c, $t = 10409$ sec), the flow transits once again into quasiperiodic motion with two fundamental frequencies, f_1 and f_2. The transition mechanism is based on the

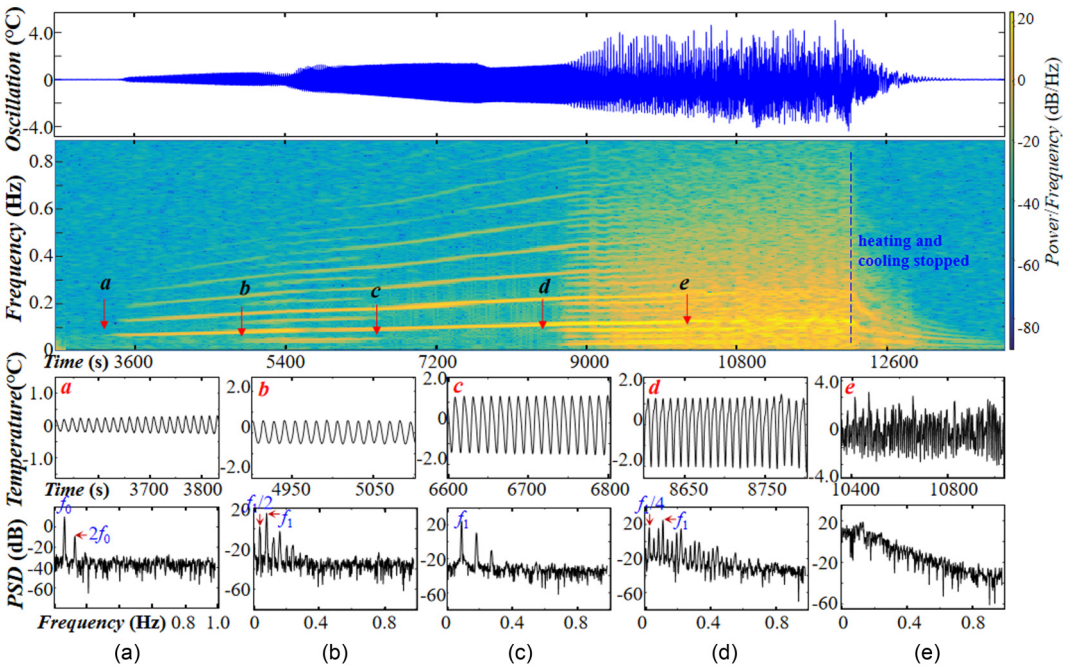

FIG. 13. Double-periodic transition route with inverse bifurcation III ($A = 1.1$; $V = 0.78$): (a) $\mathrm{Ma}^a = \mathrm{Ma_c}$, periodic oscillation; (b) $\mathrm{Ma}^b = 1.51\,\mathrm{Ma_c}$, double-periodic oscillation; (c) $\mathrm{Ma}^c = 2.01\,\mathrm{Ma_c}$, periodic oscillation; (d) $\mathrm{Ma}^d = 2.62\,\mathrm{Ma_c}$, quadruple-periodic oscillation; (e) $\mathrm{Ma}^e = 3.16\,\mathrm{Ma_c}$, chaos.

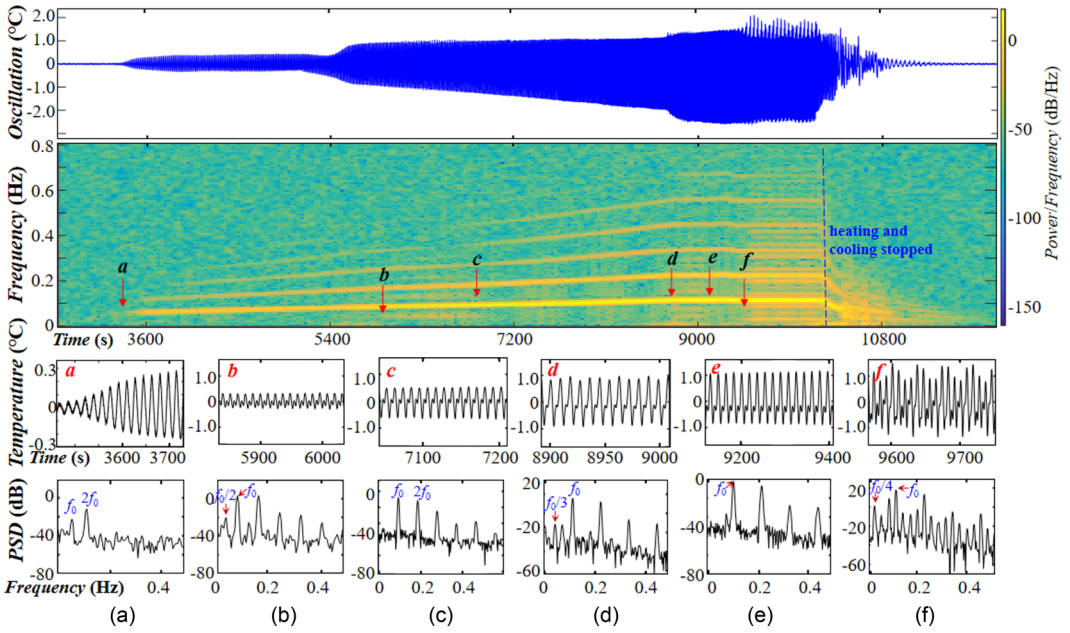

FIG. 14. Double-periodic transition route with inverse bifurcation VI ($A = 1.1$; $V = 0.80$): (a) $\mathrm{Ma}^a = \mathrm{Ma_c}$, periodic oscillation; (b) $\mathrm{Ma}^b = 1.63\,\mathrm{Ma_c}$, double-periodic oscillation; (c) $\mathrm{Ma}^c = 1.93\,\mathrm{Ma_c}$, periodic oscillation; (d) $\mathrm{Ma}^d = 2.39\,\mathrm{Ma_c}$, triple-periodic oscillation; (e) $\mathrm{Ma}^e = 2.52\,\mathrm{Ma_c}$, periodic oscillation; (f) $\mathrm{Ma}^f = 2.56\,\mathrm{Ma_c}$, quadruple-periodic oscillation.

Hopf bifurcation, with the flow gradually developing from double-periodic motion into quasiperiodic motion. As shown in Fig. 17, after two Hopf bifurcations, at $\mathrm{Ma} = 2.11\,\mathrm{Ma_c}$ (point c, $t = 7106$ sec), the fluid experiences periodic motion for a long period of time. Then, at $\mathrm{Ma} = 2.69\,\mathrm{Ma_c}$ (point d, $t = 9060$ sec), the flow transforms into double-periodic motion and then continues to bifurcate. In addition, at $\mathrm{Ma} = 2.96\,\mathrm{Ma_c}$ (point e, $t = 9969$ sec), the flow transits into sixfold-periodic oscillation and eventually enters a chaos state at $\mathrm{Ma} = 3.15\,\mathrm{Ma_c}$ (point f, $t = 10609$ sec).

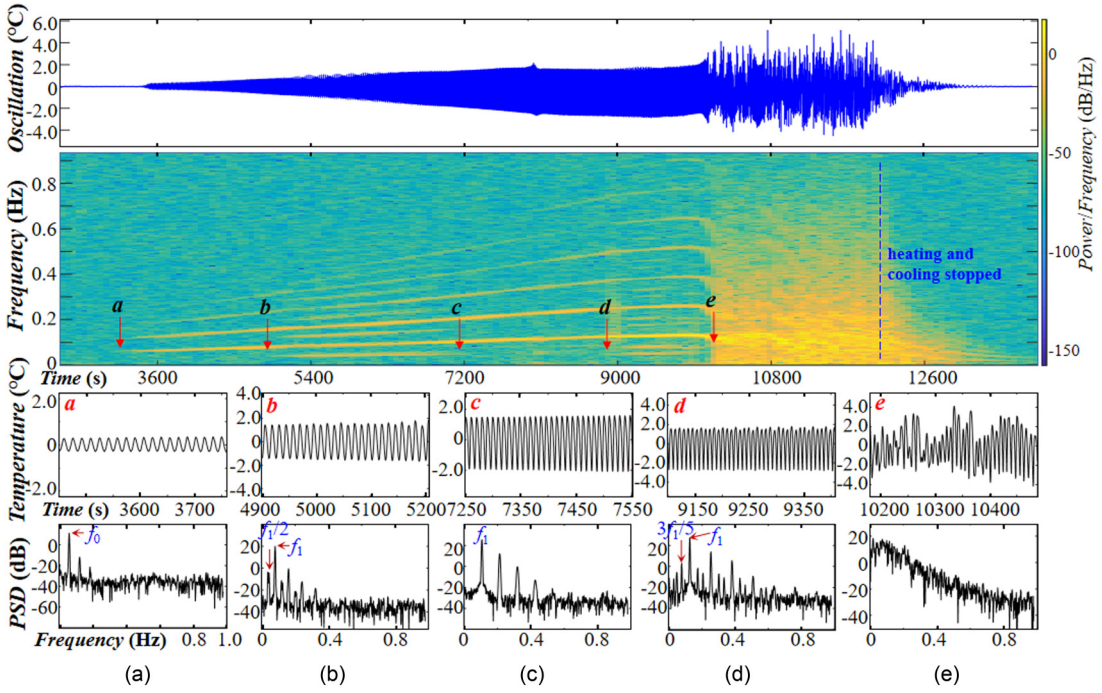

FIG. 15. Double-periodic transition route with inverse bifurcation V ($A = 1.1$; $V = 0.84$): (a) $\mathrm{Ma}^a = \mathrm{Ma_c}$, periodic oscillation; (b) $\mathrm{Ma}^b = 1.53\,\mathrm{Ma_c}$, double-periodic oscillation; (c) $\mathrm{Ma}^c = 2.27\,\mathrm{Ma_c}$, periodic oscillation; (d) $\mathrm{Ma}^d = 2.84\,\mathrm{Ma_c}$, quintuple-periodic oscillation; (e) $\mathrm{Ma}^e = 3.16\,\mathrm{Ma_c}$, chaos.

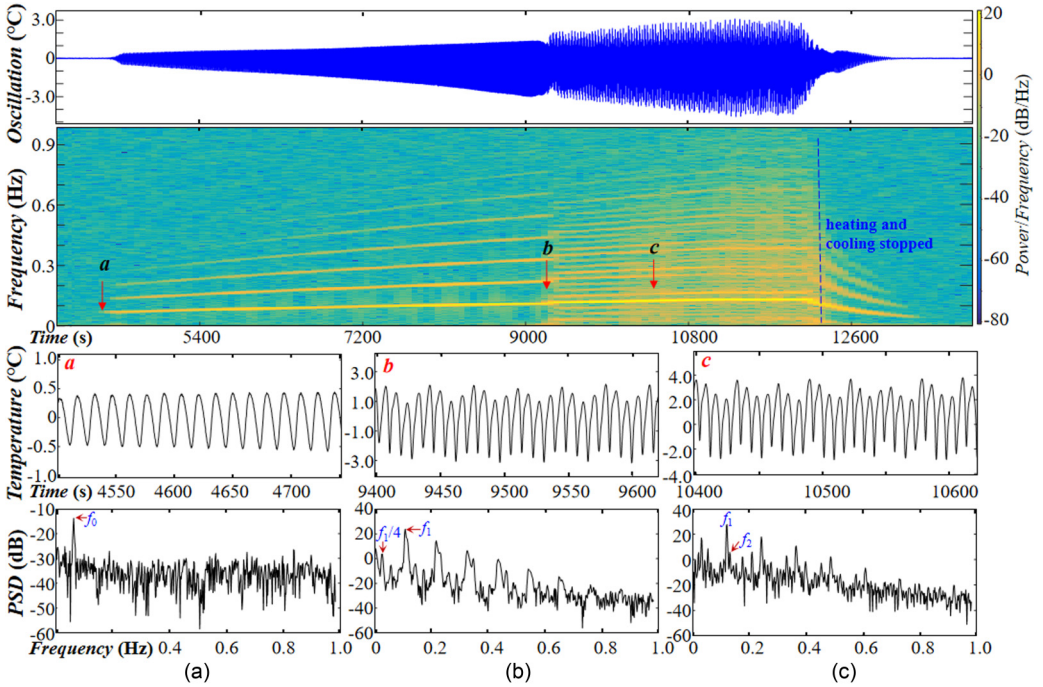

FIG. 16. Transition route coupled with quadruple-periodic oscillation and quasiperiodic oscillation ($A = 0.5$; $V = 0.96$): (a) $\mathrm{Ma}^a = \mathrm{Ma_c}$, periodic oscillation; (b) $\mathrm{Ma}^b = 2.15\,\mathrm{Ma_c}$, quadruple-periodic oscillation; (c) $\mathrm{Ma}^c = 2.33\,\mathrm{Ma_c}$, quasiperiodic oscillation with two fundamental frequencies, f_1 and f_2.

D. Intermittent transition processes

Intermittence is a widespread phenomenon observed in nature. The transition process to chaos involving intermittency is also a very typical transition route. In the time domain, the regular oscillation is suddenly "impacted" to cause chaos, and in the frequency domain, it appears as a broad band that suddenly appears or disappears, which can be clearly observed in the time-frequency diagram. Gollub and Benson and Pomeau and Manneville [18,42] initially proposed an intermittent chaos model. In the thermocapillary convection of a liquid bridge, the intermittent transition route to chaos can be commonly divided into the following three cases [42].

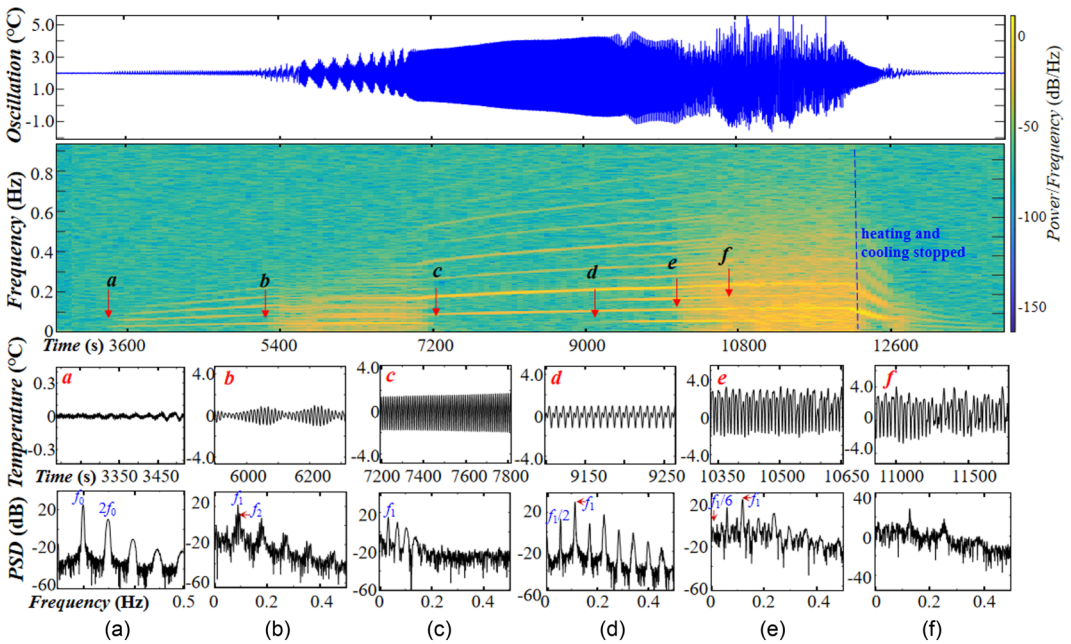

FIG. 17. Transition route coupled with double periodic oscillation, quasiperiodic oscillation and periodic oscillation ($A = 0.85$; $V = 0.70$): (a) $\mathrm{Ma}^a = \mathrm{Ma_c}$, periodic oscillation; (b) $\mathrm{Ma}^b = 1.54\,\mathrm{Ma_c}$, quasiperiodic oscillation with two fundamental frequencies, f_1 and f_2; (c) $\mathrm{Ma}^c = 2.11\,\mathrm{Ma_c}$, periodic oscillation; (d) $\mathrm{Ma}^d = 2.69\,\mathrm{Ma_c}$, double-periodic oscillation; (e) $\mathrm{Ma}^e = 2.96\,\mathrm{Ma_c}$, sixfold-periodic oscillation; (f) $\mathrm{Ma}^f = 3.15\,\mathrm{Ma_c}$, chaos.

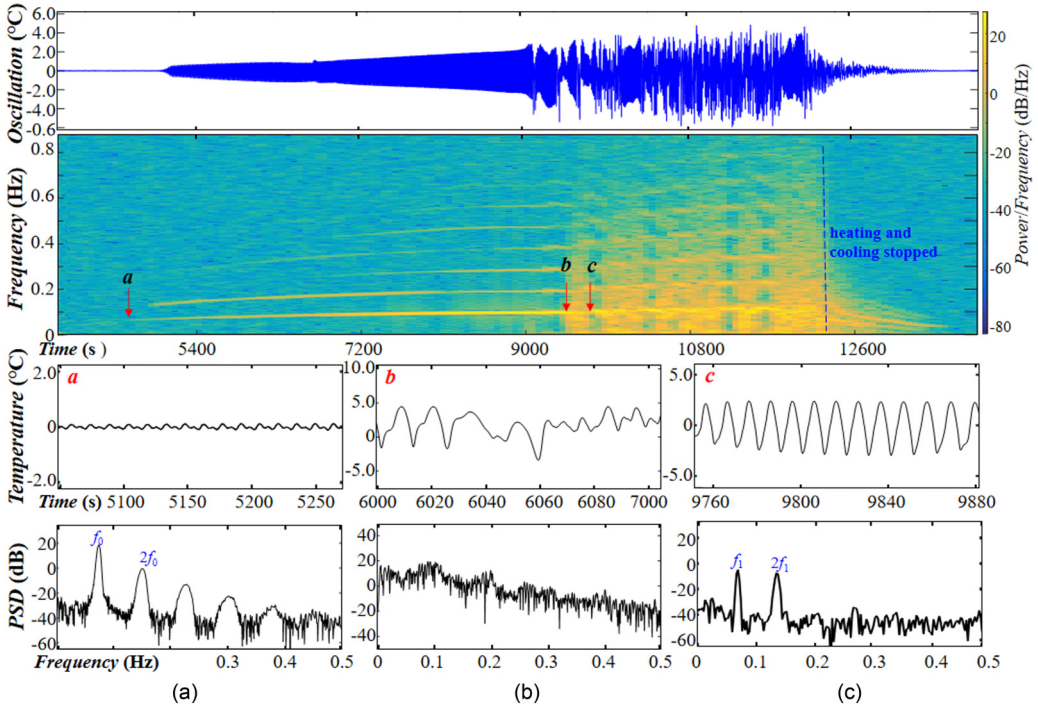

FIG. 18. Type I intermittent transition route ($A = 0.85$; $V = 0.98$): (a) $\mathrm{Ma}^a = \mathrm{Ma_c}$, periodic oscillation; (b) $\mathrm{Ma}^b = 2.01\,\mathrm{Ma_c}$, chaotic oscillation; (c) $\mathrm{Ma}^c = 2.08\,\mathrm{Ma_c}$, periodic oscillation.

Type I: Alternating state between periodic oscillation and chaos. The intermittent transition process is coupled with periodic oscillation and chaos. It can be seen in Fig. 18 that the flow loses stability to a regular periodic oscillation at $\mathrm{Ma} = \mathrm{Ma_c}$ (point a, $t = 4657$ sec). The original smooth periodic oscillation is interrupted by suddenly emerging large-amplitude chaotic fluctuations at $\mathrm{Ma} = 2.01\,\mathrm{Ma_c}$ (point b, $t = 9361$ sec), and the fluid motion switches back and forth between periodic motion and chaotic motion. With the increasing temperature differences, disordered signals appear more and more frequently, and the fluid motion becomes increasingly chaotic [18,42].

Type II: Alternating state between double-periodic oscillation and chaos. Although the mechanism is the same as that of the Type I intermittent route, chaos and period-doubling motion appear intermittently in the flow of the Type II intermittent route. It has been found that as the temperature differences increase, the subharmonic bifurcations motion suddenly weakens and the chaotic motion suddenly increases. As detailed in Fig. 19, when $\mathrm{Ma} = \mathrm{Ma_c}$ (point a, $t = 4102$ sec), the flow periodically oscillates, and its temperature oscillation amplitude gradually increases with the growing Marangoni number. However, when $\mathrm{Ma} = 2.05\,\mathrm{Ma_c}$ (point b, $t = 8409$ sec), the flow performs a quadruple-periodic motion, and the temperature oscillation amplitude descends abruptly. Meanwhile, the temperature oscillation amplitude also shows a gradually increasing trend. When $\mathrm{Ma} = 2.50\,\mathrm{Ma_c}$ (point c; $t = 10255$ sec), the flow field transits into chaos, and the above-mentioned situation is repeated. Finally, when the temperature oscillation amplitude reaches a very high value, the flow loses its regularity, and chaotic oscillation appears. The intermittent chaos and chaos caused by the period-doubling bifurcations are considered to be twin phenomena. Therefore, in principle, it is determined that in any system, if period-doubling bifurcation is observed, intermittent chaos also will be found [43].

Type III: Alternating state between quasiperiodic oscillation and chaos. This intermittent transition route is related to the Hopf bifurcation, and the transition process switches between periodic motion and quasiperiodic motion. Similar to the intermittent transition route mentioned above, its chaotic characteristics become increasingly significant [44]. As shown in Fig. 20, the flow transits from periodic motion to quasiperiodic motion because of a Hopf bifurcation. Then, as the temperature differences increase, the amplitude of the subharmonic frequency also increases. Meanwhile, the amplitude of the fundamental frequency decreases. When $\mathrm{Ma} = 2.11\,\mathrm{Ma_c}$ (point c, $t = 5754$ sec), the amplitude of the subharmonic frequency reaches a very high value. Subsequently, the signals lose regularity, and an intermittency of turbulence appears. At $\mathrm{Ma} = 2.80\,\mathrm{Ma_c}$ (point d, $t = 7636$ sec), the flow develops into a quasiperiodic state again through the Hopf bifurcation.

E. Special transition processes to chaos

Disturbances will cause a transition from laminar flow to chaos, and the disturbance can change with time and space. The transition processes are sensitive to the initial disturbance. For the flow with a small initial disturbance, the increasing disturbance wave will develop both linearly and nonlinearly. During the transition processes discussed in Secs. A to D, the transitions begin with a small-amplitude disturbance, and the amplitude of the disturbance gradually increases. When the disturbance is large enough, obvious nonlinear effects appear in the connection with more and more harmonics

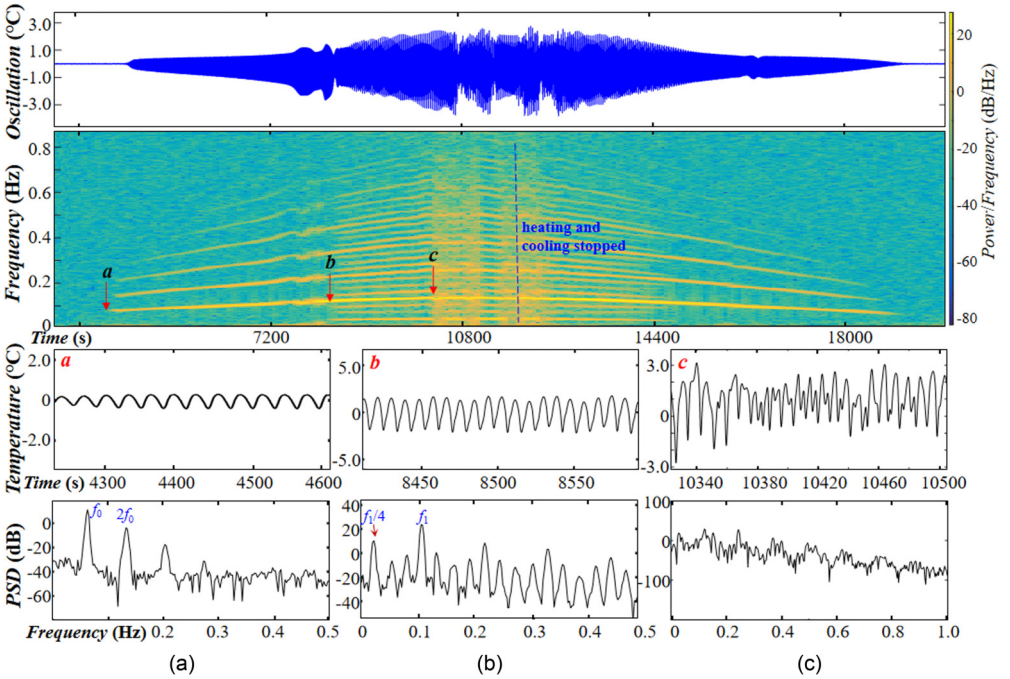

FIG. 19. Type II intermittent transition route ($A = 0.5$; $V = 1.00$): (a) $\mathrm{Ma}^a = \mathrm{Ma_c}$, periodic oscillation; (b) $\mathrm{Ma}^b = 2.05\,\mathrm{Ma_c}$, quadruple-periodic oscillation; (c) $\mathrm{Ma}^c = 2.50\,\mathrm{Ma_c}$, chaos.

being generated. Consequently, the convection will become increasingly complicated. Figures 21 and 22 show another transition process with sudden chaotic state. In Fig. 21 it can be seen that the fluid first experienced regular periodic motion in the segments *a*-*b*. Then the flow loses stability at the point *b* and directly enters chaos without any transitions or bifurcations. This is similar to flow transition processes driven by nonsurface tension in other flow systems, in which without intermediate procedures, the flow directly enters a chaotic state.

As detailed in Fig. 22, the flow transition is coupled with the time-domain oscillations and frequency-domain oscillation. It is observed that at $\mathrm{Ma} = 2.26\,\mathrm{Ma_c}$ (point b; $t =$ 24088 sec), an abrupt change in the amplitude of the tem-

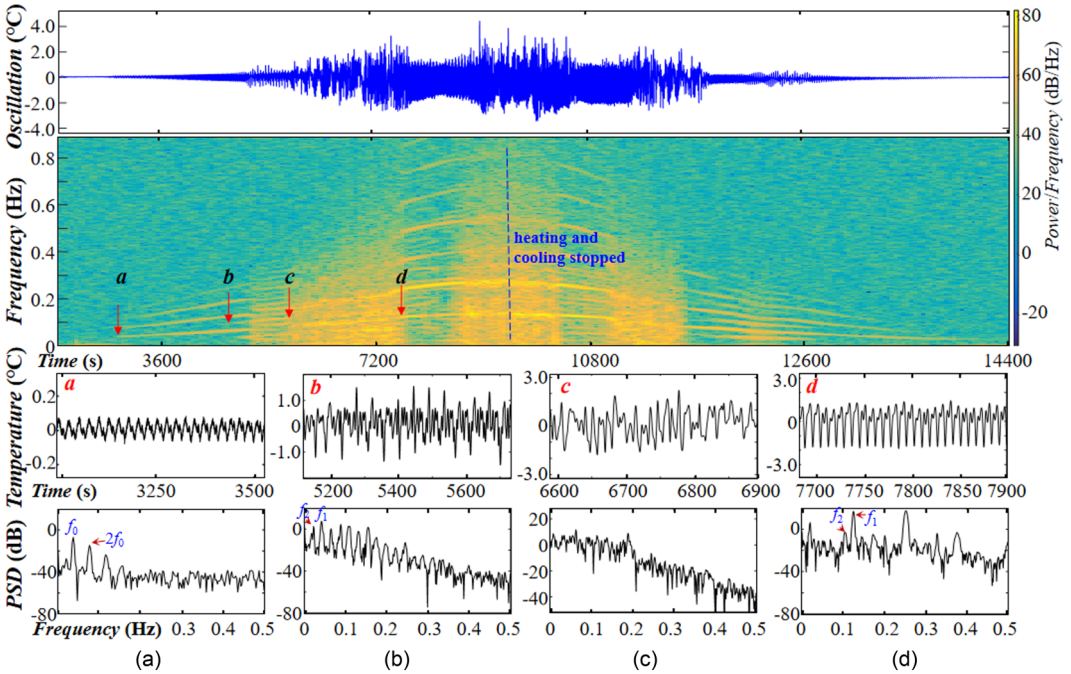

FIG. 20. Type III intermittent transition route ($A = 0.8$; $V = 0.60$): (a) $\mathrm{Ma}^a = \mathrm{Ma_c}$, periodic oscillation; (b) $\mathrm{Ma}^b = 1.75\,\mathrm{Ma_c}$, quasiperiodic oscillation with two fundamental frequencies, f_1 and f_2; (c) $\mathrm{Ma}^c = 2.11\,\mathrm{Ma_c}$, quasiperiodic oscillation with two fundamental frequencies, f_1 and f_2; (d) $\mathrm{Ma}^d = 2.80\,\mathrm{Ma_c}$, chaos.

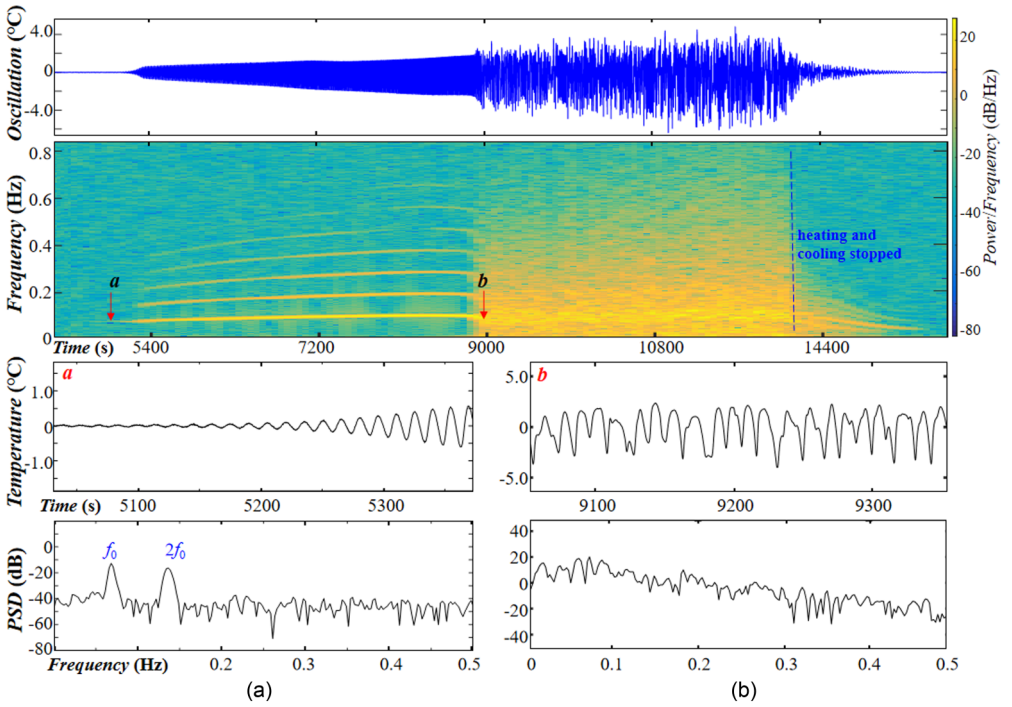

FIG. 21. One step to chaos ($A = 0.85$; $V = 0.94$): (a) $\mathrm{Ma}^a = \mathrm{Ma}_c$, periodic oscillation; (b) $\mathrm{Ma}^b = 1.88\,\mathrm{Ma}_c$, chaos.

perature signal occurred. Consequently, the flow frequency fluctuates, and the frequency curve becomes distorted. However, the frequency fluctuations will not affect the transition of the flow. At $\mathrm{Ma} = 2.62\,\mathrm{Ma}_c$ (point c; $t = 27925$ sec), subharmonic frequencies of $nf/2$, where $n = 1, 2, 3, \ldots$ emerges in the flow field. As a result, characteristics of double-periodic bifurcation are added into the flow. The two flow regimes do not interfere with each other and coexist in the transition process.

Whether the flow enters chaos from periodic motion (Fig. 21) or a fluctuation state (Fig. 22), the entire transition process of convection can be explained by the stability theory and the dissipation structure theory [18,42]. At the initial state of thermocapillary convection, since the temperature gradient is small, the convection is in a laminar state without oscillations and the flow is still in a linear regime. As the Marangoni number increases, the flow is disturbed, and the transition of convection begins. Therefore, at the beginning of the transition process, there are only simple periodic oscillations in the convection, and the flow is located in a weak nonlinear regime. With the further increase in the temperature differences ΔT, the disturbance intensifies, and the convection

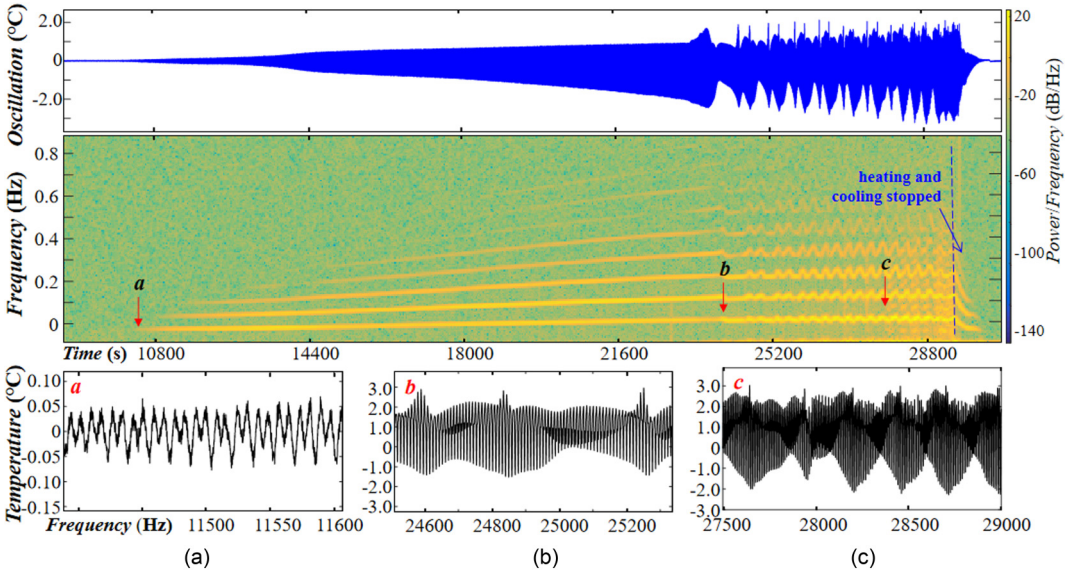

FIG. 22. Frequency oscillation transition route ($A = 0.60$; $V = 0.69$): (a) $\mathrm{Ma}^a = \mathrm{Ma}_c$, periodic oscillation; (b) $\mathrm{Ma}^b = 2.26\,\mathrm{Ma}_c$, wavy phenomenon of dominant frequency; (c) $\mathrm{Ma}^b = 2.62\,\mathrm{Ma}_c$, subharmonic frequencies of $nf/2$.

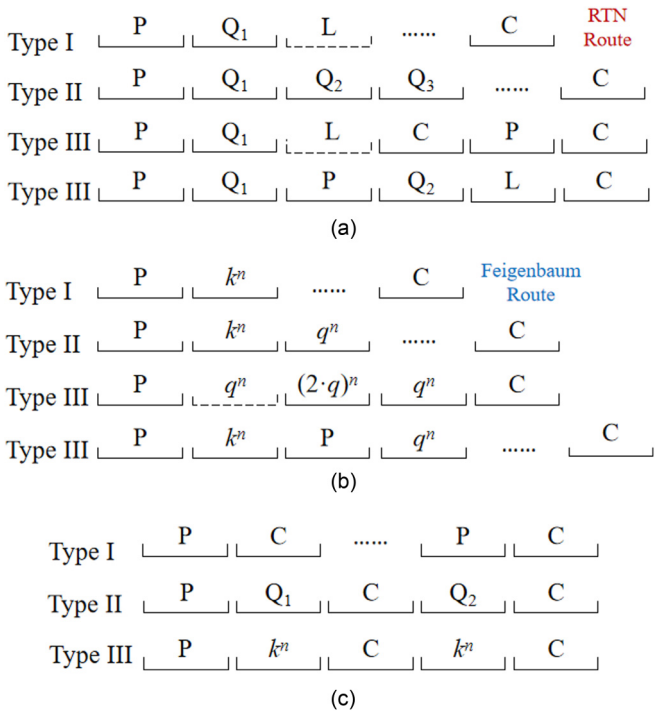

FIG. 23. Summary of transition routes to chaos: (a) quasiperiodic transition routes to chaos; (b) double periodic transition routes to chaos; (c) intermittent transition routes. P refers to the periodic oscillations; Q indicates the quasiperiodic oscillations; L represents the phase locking; k^n, q^n indicate the double-periodic oscillations, $k = 2, 3, 4, \ldots$, $q = 3, 4, 5, \ldots$; and C refers to the chaotic state.

evolves into a complex periodic oscillation state. Different frequencies will interfere with each other and also be strengthened or weakened by the weak nonlinear effects. As the disturbance continues to be amplified under weak nonlinear actions, the oscillations become chaotic and irregular, indicating that the convection has evolved into a strong nonlinear regime or chaotic state.

IV. CHAOTIC ANALYSIS OF TRANSITION ROUTES

A. Transition process analysis

To summarize the transition processes, it has been found that the flow always transitions from a steady state to periodic motion, and then evolves into a quasiperiodic motion attributed to the Hopf bifurcation [Fig. 23(a)]. However, if the quasiperiodic motion continues for a long period of time, a frequency-locking phenomenon will appear. As the coupling effects become stronger, the flow will display more obviously chaotic characteristics. Consequently, following successive bifurcation processes, it will eventually evolve into chaotic motion (Type I), which is a relatively common transition process. In these space experiments conducted in a liquid bridge, Type II to III were found to correspond to more diversified and unique transition routes. In addition, after the first Hopf bifurcation, the flow also transformed to periodic motion. However, the flow could potentially transition into quasiperiodic, periodic, or chaotic motion, and as the temperature difference increases eventually enter chaos by successive Hopf bifurcations.

In accordance with the RTN theory, provided that there are three unconventional frequencies appearing in succession, the flow will enter a state of chaos. The quasiperiodic roads involved here had not strictly met the conditions required by the RTN route to chaos, and more detailed regimes in the flow bifurcation processes were observed in the experiments. For example, in Types II to III, the quasiperiodic oscillation with two fundamental frequencies was observed to have the potential to evolve into a chaotic state after several changes of frequencies. In addition, the phenomena of frequency locking and inversion bifurcation appeared in the transition processes.

Similar to the quasiperiodic transition route, during the double-periodic bifurcation processes, a chaotic state could be obtained after successive subharmonic bifurcations, or the periodic motion or chaotic motion alternatively may continuously evolve, as detailed in Fig. 23(b). In Type III, the flow first transits from periodic motion with a fundamental frequency f_0 to a double-periodic motion with nf_1/k harmonic frequencies ($k = 2$; $n = 1, 2, 3, \ldots$), and then degenerates into a periodic motion with a new fundamental frequency f_1 through inverse bifurcation. At a later point, it bifurcates into triple-periodic motion with $nf/3$ harmonic frequencies ($nf/5$ harmonic frequencies; $n = 1, 2, 3, \ldots$; $q = 3$ or 5; and $q \neq k$), or with $f/4(k^2)$ harmonic frequencies, which were observed to change back and forth and eventually evolve into chaos. It was also found that each bifurcation in Type III was a triple-periodic motion with $nf/3$ harmonic frequencies, which indicates that $k = 3$ in $p \times k^n$ in those cases.

The intermittency mechanism is tangent bifurcations (for example, saddle knot bifurcations). It was found that regardless of Type I, Type II, or Type III intermittent transition routes, the flow transits from periodic motion to chaos owing to bifurcations. The flow state switches between regular oscillations, such as periodic, double-periodic, or quasiperiodic oscillations and irregular oscillations, and chaos. Eventually, the convection system becomes dominant and the flow evolves into complete chaos, as shown in Fig. 23(c). The fluid converges near the stable node and flows outward near the saddle point. With the increases in the Marangoni number, the fluid motion appears intermittently as a periodic state or a chaotic state, which reflects the tunnel effects of the trajectory near the critical point. The periodic motion and chaotic motion of the convection system were observed to be coupled together, leading to chaos with intermittent transitions. Details of the chaotic roads in Figs. 3–22 are summarized in Table I of the Appendix.

B. Phase space reconstruction

Phase space reconstruction is the basis for the research on chaotic time series. The nonlinear characteristics of the time series are important factors which cause a system to present chaotic phenomena. Although the time series of the thermocapillary convection system displayed a one-dimensional phenomenon in the data flow, its internal nonlinear dynamic characteristics were found to be complex. The concept of reconstruction can be introduced into the dynamic system theory by recovering or approximately simulating its potential high-dimensional dynamic environments [45]. Since the time series of a single variable output by a system can be recon-

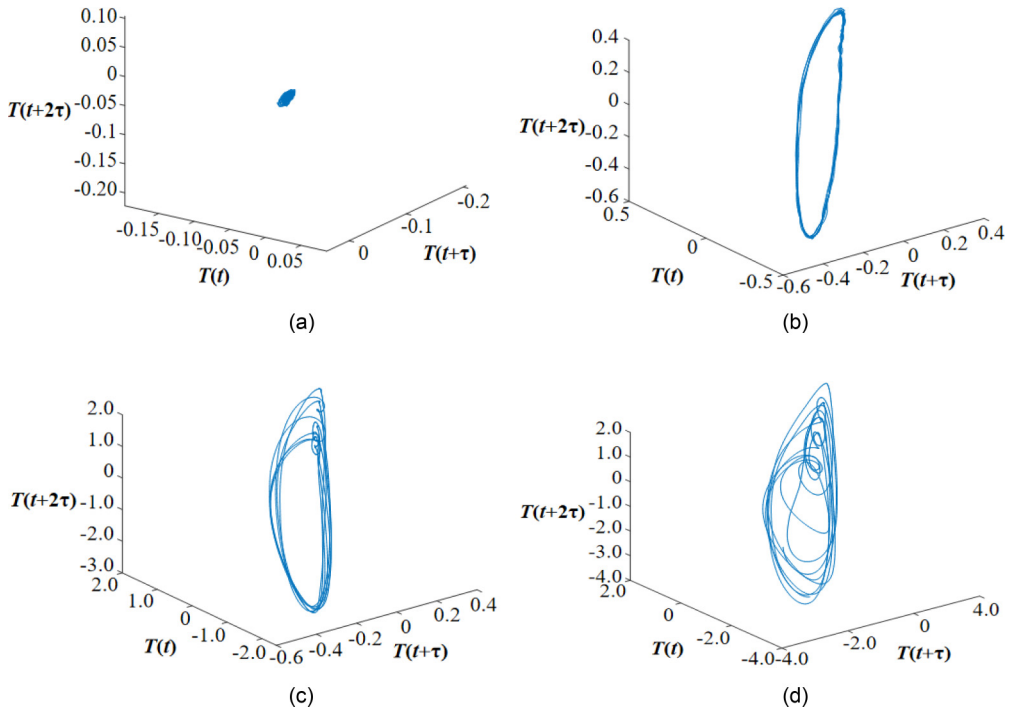

FIG. 24. Phase space reconstructions of the RTN transition process ($A = 0.6$; $V = 0.84$): (a) Ma $= 0.7\,\mathrm{Ma_c}$; (b) Ma $= \mathrm{Ma_c}$; (c) Ma $= 2.03\,\mathrm{Ma_c}$; (d) Ma $= 2.21\,\mathrm{Ma_c}$.

structed in phase space, many dynamic characteristics of the thermocapillary convection system can be obtained [14].

The reconstruction of the pseudo-phase space (PPS) was conducted from a single time series of the fully developed surface temperature by applying the time-delayed coordinates [45]. The m-dimensional coordinate was defined as follows:

$$v_m(t) = (T(t),\ T(t+\tau),\ T(t+2\tau),\ \ldots, T[t+(m-1)\tau]), \tag{4.1}$$

where T(t) represents the oscillation temperature at time t, and τ indicates the delay time.

The emergence of strange attractors indicated that the system had some instability issues. The directions of movements inside and outside the attractor had varied. It was observed that all the movements outside the singular attractor were toward (attracted to) the attractor, and they were in a "stable" direction. However, all the movements which reached the singular attractor repelled each other, and they were found to be in the "not stable" direction. That is to say, when the fundamental frequencies had close values, the movements of the attractor were characterized by mutual attraction, showing a "stable" form. However, when the fundamental frequencies had largely different values, the repulsion of the movements aggravated the "instability" of the flow system. As can be seen in Fig. 24, in the classic RTN transition route, the flow bifurcated from periodic motion to a state in which limited cycles appeared. In addition, it can be seen in the figure that the flow was affected by the bifurcation. Two-dimensional limit cycles continued to evolve, and the inner diameter of the torus continued to shrink. Meanwhile, the outer diameter and the position of the torus remained almost unchanged. When the ability of repulsion in the attractor exceeded the ability of proximity, the phase space became extremely irregular and entered chaos.

It has been determined that the shape of the torus will change with different specific flow patterns. Each Hopf bifurcation can be regarded as a change in the solution of the flow equation. During the continuous evolution process of the flow, the solution will continuously iterate in the interval. However, different from the bifurcation process shown in Fig. 24, in the bifurcation process shown in Fig. 25, due to the influencing effects of external disturbances, the iteration interval of the solution changed, which was manifested as the change in the shape of the torus. Since its transition mechanism was still the Hopf bifurcation, the entire motion trajectory still presented an attractor state, due to the fact that the orbit was never repeated and the tracking point infinitely approached the initial point. Figure 25 also shows the phase space evolution process of the transition process illustrated in Fig. 3. Its initial state was same as in the RTN route. However, during the later bifurcation process, with the further development of the flow, although the torus of the limit cycle continued to expand, the interval of the solution of the flow equation also changed. As a result, the size and position of the limit cycle were also altered. It was observed that when the two fundamental frequencies were close to each other, the band-shaped inner track formed by the torus was regular. When the two fundamental frequencies were largely different, the internal structure of the torus became more complicated due to the effects of continuous expansion.

In phase space analysis (Fig. 24), the steady motion corresponded to a fixed point; periodic motion corresponded to a limited circle; and quasiperiodic motion corresponded to a limited torus (two-dimensional torus). A torus of three dimensions or even higher dimensions (for example, a torus with at least three frequencies) chaotic motion is easily generated. According to the theory of Curry *et al.* [39],

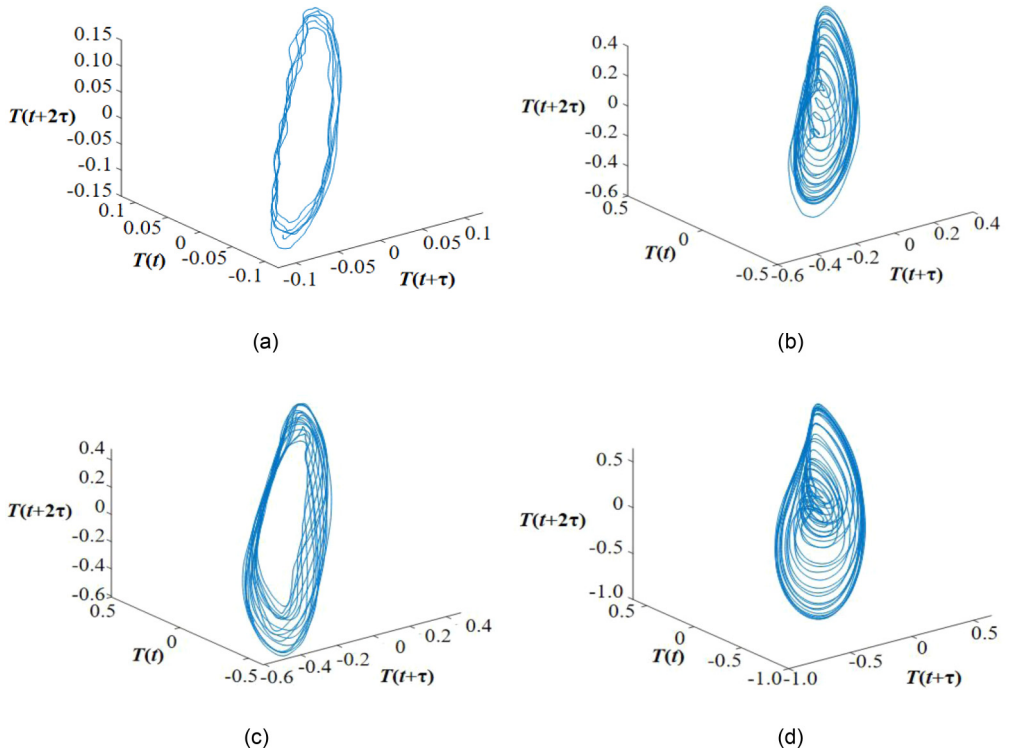

FIG. 25. Phase space reconstruction of the quasi-periodic transition process coupled with beat phenomena ($A = 0.65$; $V = 0.65$): (a) $\mathrm{Ma} = \mathrm{Ma_c}$; (b) $\mathrm{Ma} = 1.28\,\mathrm{Ma_c}$; (c) $\mathrm{Ma} = 1.52\,\mathrm{Ma_c}$; (d) $\mathrm{Ma} = 1.70\,\mathrm{Ma_c}$.

the three-dimensional torus model generated from the Hopf bifurcation was not stable. Consequently, the third incommensurate frequency could not be observed in many cases. The flow had obviously changed from counterperiodic motion to a chaotic motion on the singular attractor from a two-dimensional torus. In principle, the change also applied to the Ruelle-Takens-Newhouse two-dimensional case [19]. The quasiperiodic transitions in the liquid bridge in this space

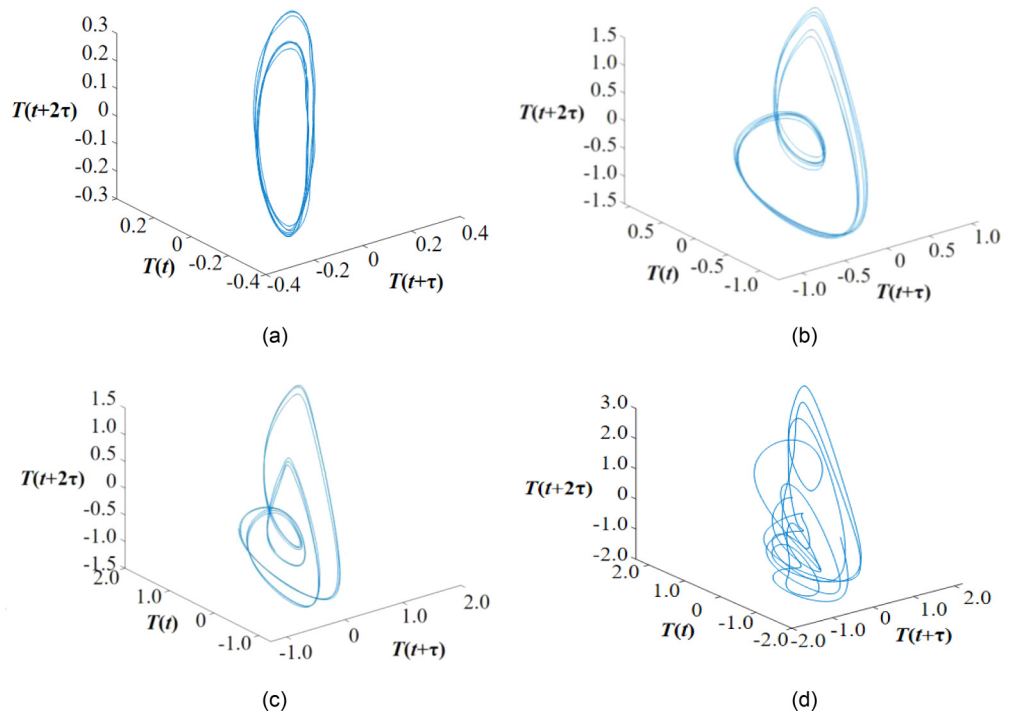

FIG. 26. Phase space reconstruction of the Feigenbaum transition process ($A = 0.65$; $V = 0.65$): (a) $\mathrm{Ma} = 1.10\,\mathrm{Ma_c}$; (b) $\mathrm{Ma} = 2.03\,\mathrm{Ma_c}$; (c) $\mathrm{Ma} = 2.25\,\mathrm{Ma_c}$; (d) $\mathrm{Ma} = 2.45\,\mathrm{Ma_c}$.

experiments had mainly taken this transition route, as shown in Fig. 3.

During the period-doubling transition process, as the flow evolved, following a bifurcation in the flow field, two similar orbital tori appeared. These displayed double-periodic oscillations at a frequency of $nf/2$ [Fig. 26(b); $n = 1, 2, 3, \ldots$]. After more bifurcations, the number of orbital tori was doubled again and again [Fig. 26(c)]. As numerous orbital tori became stacked, the flow finally entered a state of chaos, as shown in Fig. 26(d).

C. Lyapunov exponent analysis

The Lyapunov exponent is a parameter for evaluating the mean separation rate of trajectories in the phase space. In a continuous nonlinear dynamic system, the sphere will evolve to an ellipsoid, and the principal axis in the i direction is $p_i(t)$. The Lyapunov exponent in the i direction is defined as $\lambda_i = \lim_{t\to\infty} \frac{1}{t}\log_2 \frac{p_i(t)}{p_i(0)}$. If the Lyapunov exponent is larger than 0, it indicates that the system enters chaos. Many experiments show that the thermocapillary convection is sensitivity to the initial condition once the largest Lyapunov exponent $\lambda_L > 0$ [46,47].

In order to estimate the largest Lyapunov exponent from time series, we adopt the Wolf algorithm [48] and the steps are described as follows. (1) We reconstruct the one-dimensional signal into an m-dimensional phase space sequence $Y(t) = X(t), X(t+\tau), X(t+2\tau), \ldots, X(t+(m-1)\tau)$, which τ is the delay and m is the embedding dimension. (2) A neighbor of the point $Y(t_i)$ at $t = t_i$ is searched in data set $\{Y(t), t = 1, \ldots, N\}$, which is named as $Y(t')$. Then the distance between $Y(t_i)$ and its neighbor is obtained $d(t) = ||Y(t') - Y(t)||$. (3) According to the trajectories of $Y(t)$ and $Y(t')$, we predict the evolution points $Y(t+1)$ and $Y(t'+1)$ and calculate the evolution distance $d'(t) = ||Y(t+1) - Y(t'+1)||$. (4) In the next time step, a new neighbor $Y(t')$ is selected if there exists a point with a smaller distance and at the similar direction of old neighbor. Then, repeat the step (3) to start a new evolution. Finally, the largest Lyapunov exponent is estimated through the formula

$$\lambda_L(t) = \frac{1}{k\Delta t}\sum_{k=1}^{t}\log_2\frac{d'(k)}{d(k)}. \tag{4.2}$$

It should be noticed that the delay τ and embedding dimension m are important parameters when calculating the largest Lyapunov exponent. The time delay τ is determined by finding the local minimum of Average Mutual Information between $X(t)$ and $X(t+\tau)$. It means that mutual dependence between $X(t)$ and $X(t+\tau)$ is the weakest, where the phase space sequence $Y(t)$ contains the largest amount of information. The embedding dimension is estimated by the False Nearest Neighbor algorithm. This algorithm guarantees that the points in phase space contain enough information with a low dimension.

The correlation dimension can express the geometric properties of the trajectory in the phase space. A fraction of the correlation dimension proves the fractal structure of the flow system. The correlation integral is defined as

$$C(r) = \lim_{N\to\infty}\frac{1}{N(N-1)}\sum_{i,j=1,i\neq j}^{N}\theta(r - |Y(t_i) - Y(t_j)|), \tag{4.3}$$

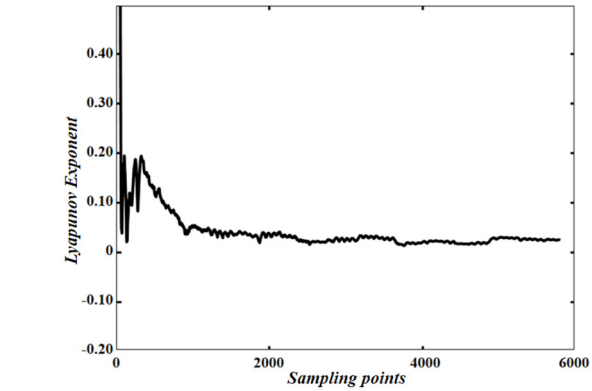

(a)

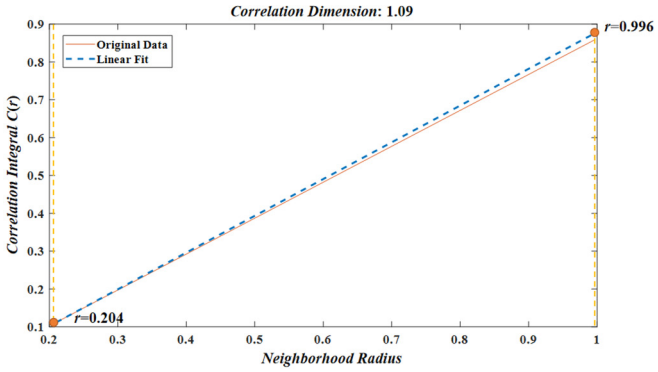

(b)

FIG. 27. Analysis of a periodic oscillation signal of Fig. 24(b) ($A = 0.85$, $V = 0.78$, $\mathrm{Ma} = 2.44\,\mathrm{Ma_c}$, 6000 data points): (a) Evolution of the Lyapunov exponent; (b) relationship between C(r) and r.

where $\theta(x)$ is the Heaviside function ($\theta = 1$ if $x \geqslant 0$, $\theta = 0$ if $x < 0$), and r is the neighborhood radius. The correlation dimension is estimated by the slope of $\ln[C(r)]$ vs $\ln(r)$.

The largest Lyapunov exponent is evaluated as one important exponent to describe the chaotic characteristics. Figure 27 shows the analysis of a periodic oscillation signal of Fig. 24(b), in which we take 6000 sampling points for analysis (300 sec). The time delay determined according to the average mutual information method is 69 sampling points, which is equal to 3.45 sec. When the calculated embedding dimension is $m = 4$ according to the false neighbor point, the proportion of the false neighbor point drops to 0.02%, which satisfies the threshold and conditions we set, $P_{\mathrm{fnn}} < P_{\mathrm{th}}$ (threshold 5%,). Figure 27(a) shows the evolution of the Lyapunov exponent calculated by the Wolf method. When the sampling points are larger than 3000, the Lyapunov exponent calculated by the Wolf method converges to the largest Lyapunov exponent λ_L. We take the average of the last 2000 evolution points (0.0232) as the largest Lyapunov exponent. Theoretically, the phase space trajectory of periodic oscillation is a limit cycle, so the maximum Lyapunov exponent is equal to zero. The oscillation obtained in the experiment is not a completely regular oscillation, as the temperature difference is slowly increasing linearly, so the amplitude of the oscillation gradually increases. Figure 27(b) indicates the relationship between the correlation integral $C(r)$ and r in double logarithmic coordi-

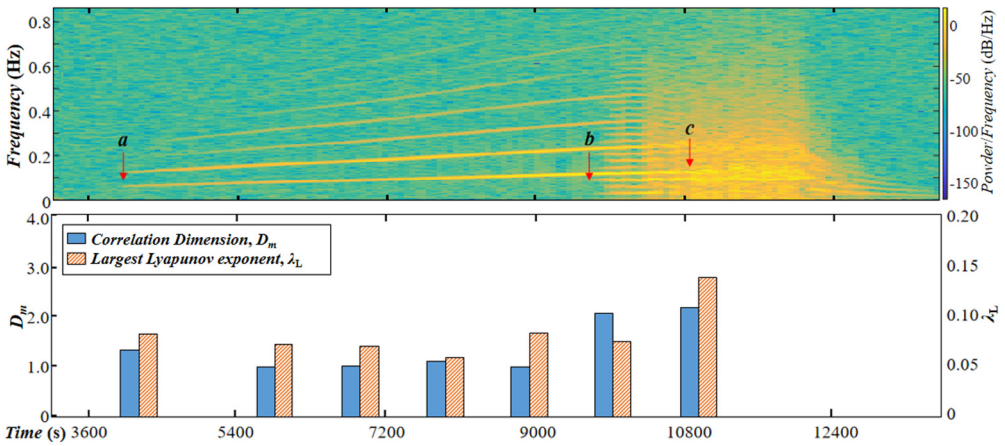

FIG. 28. Changes of the largest Lyapunov exponent (λ_L) and correlation dimension (D_m) in the quadrupled periodic transition route ($A = 0.85, V = 0.78$).

nates. The range we selected is [0.2, 0.9], and the calculated correlation dimension is 1.08, which is very close to the theoretical value of periodic oscillation.

As showed in Fig. 28 (corresponding to Fig. 9), the changes in the correlation dimension and Lyapunov exponent in the quadruple periodic oscillation transition road to chaos are given. In the periodic oscillation stage, the correlation dimension of the system is 1, and the Lyapunov exponent is close to 0 (≈0.05). It is worth noting that near the critical point, because the signal has a relative low signal-to-noise ratio (SNR), the correlation dimension and Lyapunov exponent are overestimated due to the disturbance of the noise. In the quadruple

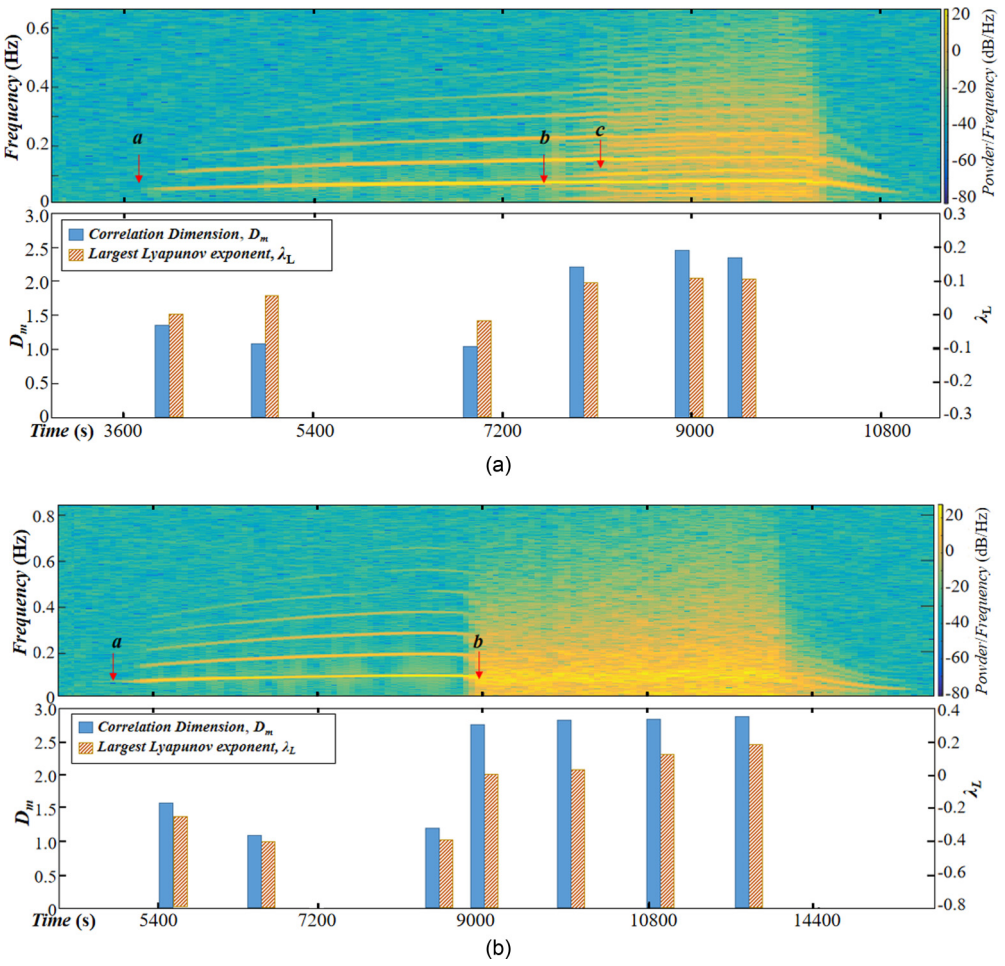

FIG. 29. Changes in characteristic quantities in different Hopf bifurcation processes: (a) RTN road to chaos; (b) one step to chaos.

periodic oscillation stage, the correlation dimension of the system jumps to 2.09, but the Lyapunov exponent is still 0.05, which is consistent with that of the periodic oscillation. Though the change of the correlation dimension indicates the transformation of the attractor's topological structure, the attractor has not entered the chaotic stage. This small positive value is mainly due to the gradual change of the oscillation state caused by the increase of the temperature difference. In the chaotic stage, an obvious broadband can be noted from the time-frequency diagram. The correlation dimension of the system is estimated to be 2.214, and the fractional dimension indicates the appearance of the strange attractor. The largest Lyapunov exponent is 0.1783, which has increased by 3.5 times compared with the previous periodic quadruple oscillation stage, and the system has entered chaos.

Figure 29(a) shows the evolution process of the correlation dimension and Lyapunov exponent on the quasiperiodic transition route (RTN route). In the periodic oscillation stage, the correlation dimension is 1, and the Lyapunov exponent is close to 0 (−0.016–0.057). When the flow becomes a quasiperiodic oscillation, the correlation dimension is 2.223–2.465, which means that the fractional dimension system occurs. The Lyapunov exponent is 0.0963–0.1105, which is double the periodic oscillation. It is demonstrated in Fig. 29(a) that once the system enters the quasiperiodic oscillation, it exhibits chaotic characteristics. Figure 29(b) shows a one-step transition road to chaos (corresponding to Fig. 21), which the system transits directly from periodic oscillation to chaos. As the frequency spectrum cannot quantitatively describe the chaotic characteristics of the system, the correlation dimension and Lyapunov exponent are helpful to detect the evolution of the strange attractor. In the chaotic state, it shows that the correlation dimension remains almost unchanged, 2.84–2.90, but the Lyapunov exponent gradually increases with the increasing temperature difference. This indicates that the topological structure of the strange attractor stays consistent, but the attractor is stretched so that the oscillation becomes more disordered.

V. CONCLUSIONS

In the present study, the transition process to chaos of thermocapillary convection in a liquid bridge on Tiangong-2 was systematically investigated. It was found that there were abundant nonlinear physical phenomena in the thermocapillary convection under microgravity conditions, and the flow was observed to have various transition routes to chaos with multiple bifurcation mechanisms.

The heat transfer process, coupled with the shear flow driven by surface tension, was the basic characteristic of the thermocapillary convection. Differing from the free surface of the complex configurations in ground environments, the liquid surface of the liquid bridge under microgravity conditions exhibited excellent axial symmetry, showing unique flow instability laws and oscillation characteristics. The classic RTN route was discovered during the quasiperiodic transition process. The coupling of the beat phenomena and the quasiperiodic oscillations resulted in the frequency of the flow becoming no longer continuous, which was different from the classic RTN route. The phenomena of the inverse bifurcations caused the quasiperiodic transition process to display reciprocating fluctuations. For the double-periodic transition process, this study not only discovered the classic Feigenbaum transition route, but also obtained other various transition routes, such as triple-periodic routes, quadruple-periodic routes, and so on, which constituted the Mandelbrot set of the thermocapillary convection transition routes [48]. The coupling of the inverted bifurcation and the double-periodic oscillations confirmed that the Feigenbaum route was an ideal model, and the route from double-periodic bifurcation to chaos was diversified. Meanwhile, it was found that the quasiperiodic oscillations and the double-periodic oscillations could also potentially coexist in a thermocapillary convection system under microgravity conditions. The research results obtained in this study successfully break through the typical bifurcation theory leading to chaos and enrich the diversity of the transition and bifurcation mechanisms of thermocapillary convection. It is determined that three types of intermittencies exist in a fluid system, which confirms the universality of the presented classification results.

It is known that bifurcation will cause sudden changes in feature quantity, leading to the reconstruction of a flow field. This study confirmed that the thermocapillary convection finally enters a chaotic state by introducing a classical chaotic dynamics theory. By the combined analysis of the largest Lyapunov exponent and the correlation dimension in the transition to chaos, we find that the attractor stays periodic during the quadrupled periodic transition while it changes to the strange attractor during the quasiperiodic transition. It is also found that the Lyapunov exponent increases while the correlation dimension is almost unchanged during the chaotic stage. It was concluded in this study that since thermocapillary convection is a typical nonlinear system, examining its transition process is of major academic value for understanding the nature of chaos.

ACKNOWLEDGMENTS

This project is supported by the China Manned Space Engineering Program. Many participants have contributed to the work reported in this project. We would like to express our great appreciation to the Payload Operation and Application Center (POAC) for their services and assistances in formulating and sending space experiment command.

APPENDIX

Figure 30 is the distribution of the transition routes involved in the present work on the aspect ratio to volume ratio. Figure 31(a) is a graph showing the relationship between the critical frequency and the aspect ratio, and Fig. 31(b) is a graph showing the relationship between the critical frequency and the volume ratio. It can be seen from the figures that both the aspect ratio and the volume ratio affect the transition route and the critical frequency. As the height of the liquid bridge increases, the critical frequency decreases, which is consistent with previous work [35]. The fundamental critical frequency

TABLE I. Details of Figs. 3–22.

Fig	A	V	f_0	f_1, f_2 (f/n)	...			Observed states
3	0.6	0.84	**Ma_c:** $f_0 = 0.054$ Hz	**2.03 Ma_c:** $f_1 = 0.078$ Hz, $f_2 = 0.110$ Hz	**2.21 Ma_c:** $f_1 = 0.080$ Hz, $f_2 = 0.115$ Hz, $f_3 = 0.047$ Hz			P Q(f_1, f_2) Q(f_1, f_2, f_3)
4	0.4	0.45	**Ma_c:** $f_0 = 0.098$ Hz	**1.28 Ma_c:** $f_1 = 0.111$ Hz, $f_2 = 0.153$ Hz	**1.47 Ma_c:** $f_1 = 0.149$ Hz, $f_2 = 0.157$ Hz	**1.66 Ma_c:** $f_1 = 0.161$ Hz, $f_2 = 0.184$ Hz		P Q(f_1, f_2) Q(f_1, f_2) Q(f_1, f_2)
5	1.1	6.6	**Ma_c:** $f_0 = 0.034$ Hz	**1.37 Ma_c:** $f_1 = 0.059$ Hz, $f_2 = 0.068$ Hz	**1.64 Ma_c:** $f_1 = 0.061$ Hz	**2.71 Ma_c:** $f_1 = 0.093$ Hz, $f_2 = 0.110$ Hz	**3.43 Ma_c:** C	P Q(f_1, f_2) P Q(f_1, f_2) C
6	1.1	0.56	**Ma_c:** $f_0 = 0.027$ Hz	**1.73 Ma_c:** $f_1 = 0.041$ Hz, $f_2 = 0.027$ Hz	**2.28 Ma_c:** C	**3.67Ma_c:** $f_1 = 0.056$ Hz	**4.50 Ma_c:** C	P Q(f_1, f_2) C P C
7	0.65	0.65	**Ma_c:** $f_0 = 0.068$ Hz	**1.89 Ma_c:** $f_1 = 0.117$ Hz, $f_1/2 = 0.059$ Hz	**1.98 Ma_c:** $f_1 = 0.117$ Hz, $f_1/4 = 0.029$ Hz, $3f_1/4 = 0.088$ Hz	**2.07Ma_c:** Cs		P $k^n(f/2)$ $k^n(f/4)$ C
8	0.95	0.94	**Ma_c:** $f_0 = 0.062$ Hz	**2.38Ma_c:** $f_1 = 0.131$ Hz, $f_1/3 = 0.044$ Hz, $2f_1/3 = 0.087$ Hz	**2.61Ma_c:** C			P $q^n(f/3)$ C
9	0.85	0.78	**Ma_c:** $f_0 = 0.093$ Hz	**2.44Ma_c:** $f_1 = 0.116$ Hz, $f_1/4 = 0.029$ Hz, $3f_1/4 = 0.087$ Hz	**2.71Ma_c:** C			P $q^n(f/4)$ C
10	0.5	0.70	**Ma_c:** $f_0 = 0.098$ Hz	**2.19Ma_c:** $f_1 = 0.100$ Hz, $f_1/4 = 0.025$ Hz, $3f_1/4 = 0.075$ Hz	**2.36Ma_c:** $f_1 = 0.103$ Hz, $f_1/5 = 0.021$ Hz, $4f_1/5 = 0.082$ Hz			P $q^n(f/4)$ $q^n(f/5)$
11	0.95	0.98	**Ma_c:** $f_0 = 0.064$ Hz	**2.12Ma_c:** $f_1 = 0.124$ Hz, $f_1/3 = 0.041$ Hz, $2f_1/3 = 0.083$ Hz	**2.33Ma_c:** $f_1 = 0.129$ Hz, $f_1/6 = 0.022$ Hz, $f_1/3 = 0.043$ Hz	**2.49Ma_c:** $f_1 = 0.102$ Hz, $f_1/3 = 0.035$ Hz, $2f_1/3 = 0.035$ Hz	**2.63Ma_c:** C	P $q^n(f/3)$ $q^n(f/6)$ $q^n(f/3)$ C
12	0.85	0.70	**Ma_c:** $f_0 = 0.072$ Hz	**2.06Ma_c:** $f_1 = 0.115$ Hz, $f_1/3 = 0.038$ Hz, $f_1/2 = 0.057$ Hz, $2f_1/3 = 0.077$ Hz	**2.22Ma_c:** $f_1 = 0.123$ Hz, $f_1 3 = 0.041$ Hz, $2f_1/3 = 0.082$ Hz	**2.34Ma_c:** C		P $q^n(f/6)$ $q^n(f/3)$ C
13	1.1	0.80	**Ma_c:** $f_0 = 0.061$ Hz	**1.51Ma_c:** $f_1 = 0.077$ Hz, $f_1/2 = 0.038$ Hz	**2.01Ma_c:** $f_1 = 0.088$ Hz	**2.62Ma_c:** $f_1 = 0.111$ Hz, $f_1/4 = 0.027$ Hz, $3f_1/4 = 0.084$ Hz	**3.16Ma_c:** C	P $q^n(f/2)$ $q^n(f/3)$ C
14	1.1	0.80	**Ma_c:** $f_0 = 0.059$ Hz	**1.63Ma_c:** $f_1 = 0.083$ Hz, $f_1/2 = 0.041$ Hz	**1.93Ma_c:** $f_1 = 0.093$ Hz	**2.39Ma_c:** $f_1 = 0.112$ Hz, $f_1/3 = 0.037$ Hz, $2f_1/3 = 0.075$ Hz	**2.52Ma_c:** $f_1 = 0.112$ Hz	**2.56Ma_c:** $f_1 = 0.110$, $f_1/4 = 0.027$ Hz, $f_1/2 = 0.055$ Hz, $3f_1/4 = 0.083$ Hz	P $q^n(f/2)$ P $q^n(f/3)$ P $q^n(f/4)$
15	1.1	0.84	**Ma_c:** $f_0 = 0.061$ Hz	**1.53Ma_c:** $f_1 = 0.081$ Hz, $f_1/2 = 0.041$ Hz	**2.27Ma_c:** $f_1 = 0.101$ Hz	**2.62Ma_c:** $f_1 = 0.126$ Hz, $2f_1/5 = 0.050$ Hz, $3f_1/5 = 0.076$ Hz	**3.16Ma_c:** C	P $q^n(f/2)$ P $q^n(f/5)$ C

TABLE I. (*Continued.*)

Fig	A	V	f_0	f_1, f_2 (f/n)	…				Observed states
16	0.5	0.96	**Ma_c:** $f_0 = 0.073$ Hz	**2.15Ma_c:** $f_1 = 0.115$ Hz, $f_1/4 = 0.029$ Hz, $f_1/2 = 0.057$ Hz, $3f_1/4 = 0.86$ Hz	**2.33Ma_c:** $f_1 = 0.123$ Hz, $f_2 = 0.156$ Hz				P $q^n(f/4)$ Q(f_1, f_2)
17	0.85	0.70	**Ma_c:** $f_0 = 0.035$ Hz	**1.54Ma_c:** $f_1 = 0.052$ Hz, $f_2 = 0.065$ Hz	**2.11Ma_c:** $f_1 = 0.101$ Hz	**2.69Ma_c:** $f_1 = 0.123$ Hz, $f_1/2 = 0.067$ Hz	**2.96Ma_c:** $f_1 = 0.128$ Hz, $f_1/6 = 0.021$ Hz, $2f_1/3 = 0.085$ Hz, $5f_1/6 = 0.107$ Hz	**3.15Ma_c:** C	P Q(f_1, f_2) P $k^n(f/2)$ $q^n(f/6)$ C
18	0.85	9.58	**Ma_c:** $f_0 = 0.061$ Hz	**2.01Ma_c:** C	**2.08Ma_c:** $f_1 = 0.095$ Hz				P C P C … …
19	0.5	1.00	**Ma_c:** $f_0 = 0.068$ Hz	**2.05Ma_c:** $f_1 = 0.113$ Hz, $f_1/4 = 0.028$ Hz, $f_1/2 = 0.057$ Hz, $3f_1/4 = 0.085$ Hz	**2.50Ma_c:** C				P $q^n(f/4)$ C $q^n(f/4)$ C
20	0.8	0.60	**Ma_c:** $f_0 = 0.038$ Hz	**1.75Ma_c:** $f_1 = 0.043$ Hz, $f_2 = 0.023$ Hz	**2.11Ma_c:** C	**2.80Ma_c:** $f_1 = 0.126$ Hz, $f_2 = 0.105$ Hz			P Q(f_1, f_2) C Q(f_1, f_2) C
21	0.85	0.94	**Ma_c:** $f_0 = 0.068$ Hz	**1.88Ma_c:** C					P C
22	0.6	0.69	**Ma_c:** $f_0 = 0.056$ Hz	**2.26Ma_c:** Wavy phenomenon of dominant frequency(WF)	**2.62Ma_c:** Subharmonic frequencies of $nf/2$				P WF k^n

For example: P: (a) of FIG. 3–22; Q: FIG. 3. (b-c) and FIG. 4. (b-d); k^n: FIG. 7. (b-c); q^n: FIG. 8. (b) and FIG. 11. (b-d).

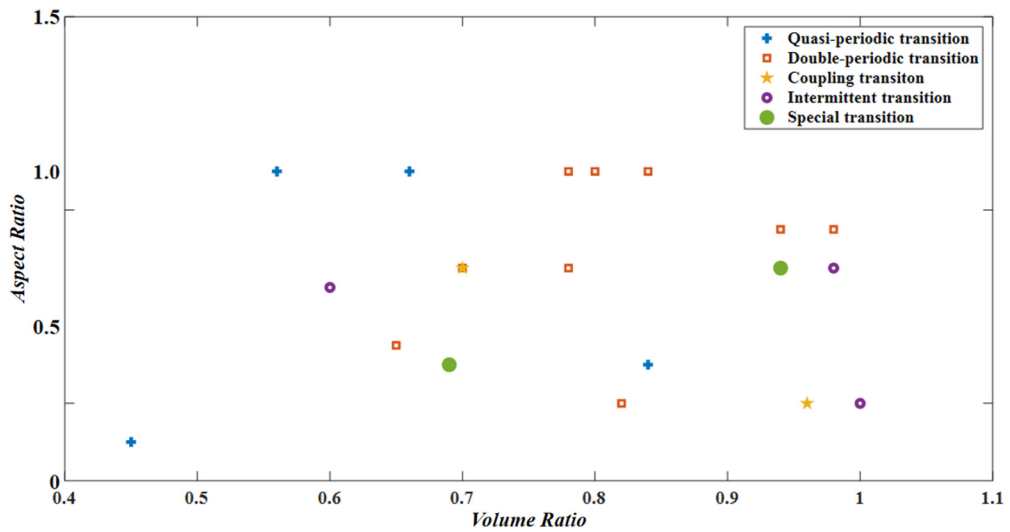

FIG. 30. Distribution of transition route in aspect ratio and volume ratio.

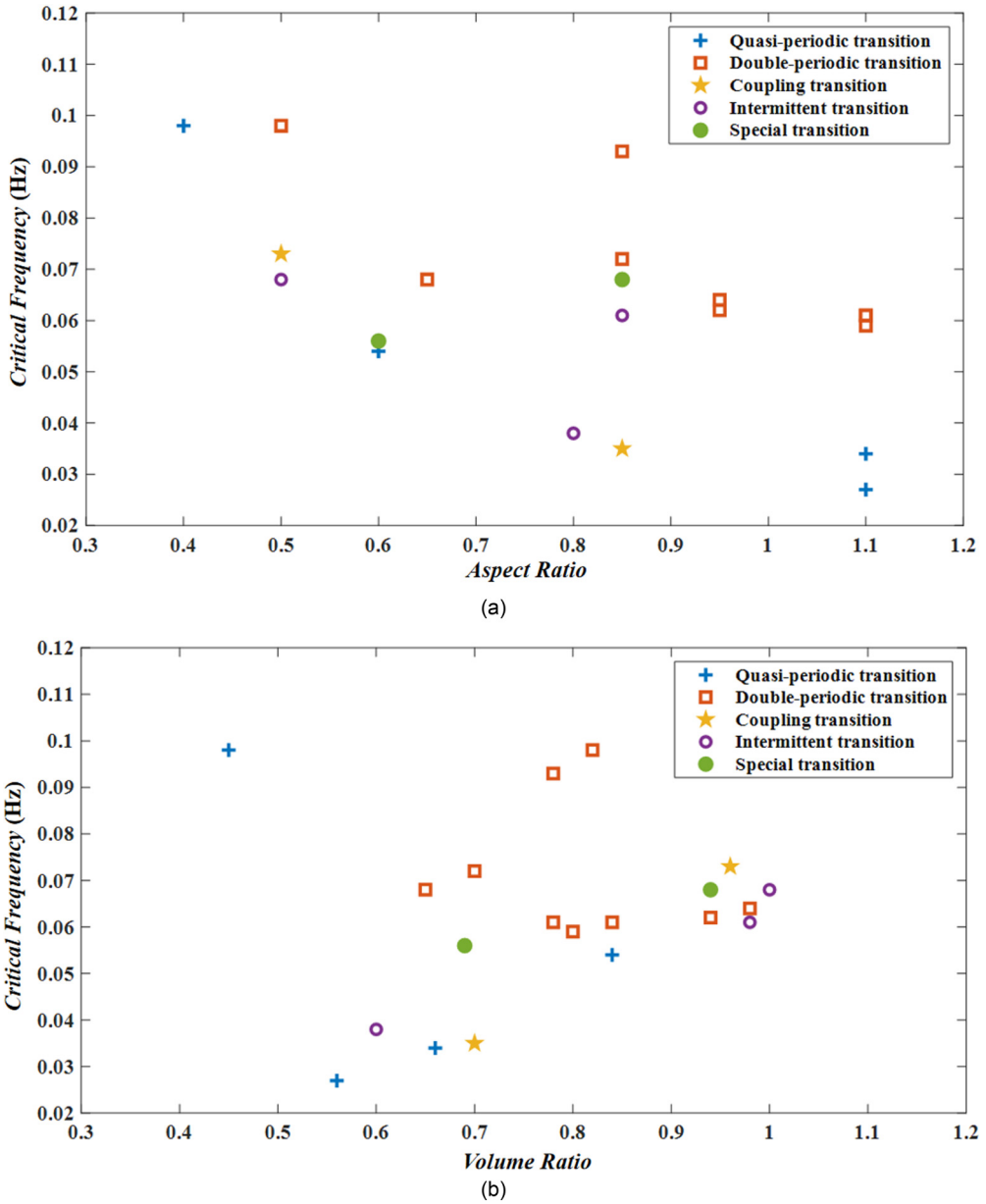

FIG. 31. Effect of geometric parameters on critical frequency, (a) the relationship between the critical frequency and the aspect ratio; (b) relationship between the critical frequency and the volume ratio.

of the double-periodic road is higher, and the critical fundamental frequency of the quasiperiodic road is lower. One step to chaos and type I of intermittent transition route are both transits from periodic oscillation to chaos, and their critical frequencies are also at a higher level. The type III road of intermittent transition and coupling transition road is affected by the quasiperiod, and the corresponding critical frequency is generally small.

[1] D. Schwabe, A. Scharmann, F. Preisser, and R. Oeder, Experiments on surface tension driven flow in floating zone melting, J. Cryst. Growth **43**, 305 (1987).

[2] C. H. Chun and W. Wuest, Experiments on the transition from the steady to the oscillatory Marangoni-convection of a floating zone under reduced gravity effect, Acta Astronaut. **6**, 1073 (1979).

[3] F. M. Schatz and G. P. Neitzel, Experiments on thermocapillary instabilities, Annu. Rev. Fluid Mech. **33**, 93 (2001).

[4] W. R. Hu, Z. M. Tang, and K. Li, Thermocapillary convection in floating zones, Appl. Mech. Rev. **61**, 010803 (2008).

[5] J. J. Xu and S. H. Davis, Convective thermocapillary instabilities in liquid bridges, Phys. Fluids **27**, 1102 (1984).

[6] D. Schwabe, Hydrothermal waves in a liquid bridge with aspect ratio near the Rayleigh limit under microgravity, Phys. Fluids **17**, 112104 (2005).

[7] T. Yano and K. Nishino, Effect of liquid bridge shape on the oscillatory thermal Marangoni convection, Eur. Phys. J. Special Topics **224**, 289 (2015).

[8] V. Shevtsova, D. Melnikov, and A. Nepomnyashchy, New Flow Regimes Generated by Mode Coupling in Buoyant-Thermocapillary Convection, Phys. Rev. Lett. **102**, 134503 (2009).

[9] D. Melnikov and V. Shevtsova, Origin of axially running waves in liquid bridges, Microgr. Sci. Tech. **21**, 53 (2009).

[10] L. Duan, Y. Yin, J. Wang, Q. Kang, D. Wu, H. Jiang, P. Zhang, and L. Hu, Thermocapillary convection space experiment on the SJ-10 recoverable satellite, JoVE **157**, e59998 (2020).

[11] R. Lavalley, G. Amberg, and H. Alfredsson, Experimental and numerical investigation of nonlinear thermocapillary oscillations in an annular geometry, Eur. J. Mech.-B/Fluids **20**, 771 (2001).

[12] C. H. Chun, Experiments on steady and oscillatory temperature distribution in a floating zone due to the Marangoni convection, Acta Astron. **7**, 4 (1980).

[13] S. Frank and D. Schwabe, Temporal and spatial elements of thermocapillary convection in floating zones, Exp. Fluids **23**, 234 (1997).

[14] I. Ueno, S. Tanaka, and H. Kawamura, Oscillatory and chaotic thermocapillary convection in a half-zone liquid bridge, Phys. Fluids **15**, 408 (2003).

[15] T. Watanabe, D. E. Melnikov, T. Matsugase, V. Shevtsova, and I. Ueno, The stability of a thermocapillary-buoyant flow in a liquid bridge with heat transfer through the interface, Microgr. Sci. Tech. **26**, 17 (2014).

[16] V. Yasnou, Y. Gaponenko, A. Mialdun, and V. Shevtsova, Influence of a coaxial gas flow on the evolution of oscillatory states in a liquid bridge, Int. J. Heat Mass Transfer **123**, 747 (2018).

[17] B. Edoardo and M. Daniela, Horizontal thermal convection of succinonitrile: Steady state, instabilities, and transition to chaos, Phys. Rev. E **69**, 056319 (2004).

[18] J. Gollub and S. Benson, Many routes to turbulent convection, J. Fluid Mech. **100**, 449 (1980).

[19] S. Newhouse, D. Ruelle, and F. Takens, Occurrence of strange Axiom *A* attractors near quasi periodic flows on T^m, $m \geqq 3$, Commun. Math. Phys. **64**, 35 (1978).

[20] L. D. Landau, On the problem of turbulence, *Collected Papers of L. D. Landau*, edited by D. Ter Haar (Pergamon Press, Oxford, 1965), pp. 387–391.

[21] B. L. Smorodin and A. V. Taraut, Dynamics of electroconvective wave flows in a modulated electric field, J. Exp. Theor. Phys. **118**, 158 (2014).

[22] B. Smorodin, B. I. Myznikova, and J. C. Legros, Evolution of convective patterns in a binary-mixture layer subjected to a periodical change of the gravity field, Phys. Fluids **20**, 094102 (2008).

[23] H. Kawamura, K. Nishino, S. Mastumoto, and I. Ueno, Report on microgravity experiments of Marangoni convection aboard International Space Station, J. Heat Transfer ASME **134**, 031005 (2012).

[24] Y. S. Li, Z. W. Chen, and J. M. Zhan, Double-diffusive Marangoni convection in a rectangular cavity: Transition to chaos, Int. J. Heat Mass Transfer **53**, 5223 (2010).

[25] S. Rahal, P. Cerisier, and C. Abid, Transition to chaos via the quasi-periodicity and characterization of attractors in confined Bénard–Marangoni convection, Eur. Phys. J. B **59**, 509 (2007).

[26] P. Zhu, L. Duan, and Q. Kang, Transition to chaos in thermocapillary convection, Int. J. Heat Mass Transfer **57**, 457 (2013).

[27] Q. Kang, H. Jiang, L. Duan, C. Zhang, and W. R. Hu, The critical condition and oscillation-transition characteristics of thermocapillary convection in the space experiment on SJ-10 satellite, Int. J. Heat Mass Transfer **135**, 479 (2019).

[28] Q. Kang, J. Wang, L. Duan, Y. Y. Su, J. W. He, D. Wu, and W. R. Hu, The volume ratio effect on flow patterns and transition processes of thermocapillary convection, J. Fluid Mech. **868**, 560 (2019).

[29] Z. M. Tang and W. R. Hu, Fractal features of oscillatory convection in the half-floating zone, Int. J. Heat Mass Transfer **38**, 3295 (1995).

[30] D. E. Melnikov, V. M. Shevtsova, and J. C. Legros, Onset of temporal aperiodicity in high Prandtl number liquid bridge under terrestrial conditions, Phys. Fluids **16**, 1746 (2004).

[31] Y. Gaponenko, V. Yasnou, A. Mialdun, A. Nepomnyashchy, and V. Shevtsova, Hydrothermal waves in a liquid bridge subjected to a gas stream along the interface, J. Fluid Mech. **908**, A34 (2020).

[32] Y. Aa, K. Li, Z. M. Tang, Z. H. Cao, and W. R. Hu, Period-doubling bifurcations of the thermocapillary convection in a floating half zone, Sci. China: Phys. Mech. Astron. **53**, 9 (2010).

[33] J. Wang, L. Duan, and Q. Kang, Oscillatory and chaotic buoyant-thermocapillary convection in the large-scale liquid bridge, Chin. Phys. Lett. **34**, 074703 (2017).

[34] T. Matsugase, I. Ueno, K. Nishino, M. Ohnishi, M. Sakurai, S. Matsumoto, and H. Kawamura, Transition to chaotic thermocapillary convection in a half zone liquid bridge, Int. J. Heat Mass Transfer **89**, 903 (2015).

[35] Q. Kang, D. Wu, L. Duan, J. Zhang, B. Zhou, J. Wang, Z. Y. Han, L. Hu, and W. R. Hu, The effects of geometry and heating rate on thermocapillary convection in the liquid bridge, J. Fluid Mech. **881**, 951 (2019).

[36] Q. Kang, D. Wu, L. Duan, L. Hu, J. Wang, P. Zhang, and W. R. Hu, Space experimental study on wave modes under instability of thermocapillary convection in liquid bridges on Tiangong-2, Phys. Fluids **32**, 034107 (2020).

[37] A. Libchaber, S. Fauve, and C. Laroche, Two-parameter study of the routes to chaos, Physica D: Nonlin. Phenom. **7**, 73 (1983).

[38] S. Martin, H. Leber, and W. Martienssen, Oscillatory and Chaotic States of the Electrical Conduction in Barium Sodium Niobate Crystals, Phys. Rev. Lett. **53**, 303 (1984).

[39] J. Curry and J. Yorke, *A Transition from Hopf Bifurcation to Chaos*, Lecture Notes in Mathematics (Springer, New York, 1987), Vol. 668.

[40] S. Paul, P. Wahi, and M. K. Verma, Bifurcations and chaos in large-Prandtl number Rayleigh–Bénard convection, Int. J. Non-Linear Mech. **46**, 772 (2011).

[41] Y. Pomeau and P. Manneville, Intermittent transition to turbulence in dissipative dynamical systems, Commun. Math. Phys. **74**, 189 (1980).

[42] D. Y. Tang, J. Pujol, and C. O. Weiss, Type-III intermittency of a laser, Phys. Rev. A **44**, R35(R) (1991).

[43] H. G. Schuster, *Deterministic Chaos: An Introduction* (Wiley-VCH, Weinheim, 1984), p. 87.

[44] M. T. Rosenstein, J. J. Gollins, and C. J. D. Luca, A practical method for calculating largest Lyapunov exponents from small data sets, Physica D **65**, 117 (1993).

[45] J. Thompson and H. Stewart, *Nonlinear Dynamics and Chaos: Geometrical Methods for Engineers and Scientists* (John Wiley & Sons, West Sussex, 2002), p. 392.

[46] W. Caesarendra, P. Kosasih, K. Tieu, and C. Moodie, An application of nonlinear feature extraction—A case study for low speed slewing bearing condition monitoring and prognosis, in *IEEE/ASME International Conference on Advanced Intelligent Mechatronics: Mechatronics for Human Wellbeing* (2013), p. 6584344.

[47] H. O. Peitgen and P. H. Richter, *The Beauty of Fractals: Images of Complex Dynamical Systems* (Springer-Verlag, Berlin, Heidelberg, 1988), p. 327.

[48] A. Wolf, J. B. Swift, H. L. Swinney, and J. A. Vastano, Determining Lyapunov exponents from a time series, Physica D **16**, 285 (1985).